Politecnico di Torino

Master's Degree in
Communications and Computer Networks Engineering

Study of high sensitivity GNSS receivers for space applications and lunar missions

Supervisors
Prof. Fabio DOVIS
Dr. Alex MINETTO

Candidate
Salvatore GUZZI

Academic Year 2021/2022

Abstract

Experimentally validating the use of in-orbit Global Navigation Satellite Systems (GNSS) receivers within the Space Service Volume (SSV) has been accomplished at LEO, MEO, and GEO altitudes respectively. Therefore, the most recent missions have revealed the GNSS performance at distances of approximately 150,000 kilometers away from the surface of the Earth. The study of Earth GNSS signals beyond such an altitude is still a matter of research, and it is primarily based on modeling and extrapolation from the experience of using GNSS on both the surface of the Earth and on lower orbits. The Lunar GNSS Receiver Experiment (LuGRE) is a payload that will be carried by the Firefly Blue Ghost Mission 1 and will be a joint effort between NASA and the Italian Space Agency (ASI). Its purpose is to demonstrate GNSS-based positioning, navigation, and timing on the Moon. After its launch in 2024, the LuGRE spacecraft will collect GPS and Galileo measurements while traveling between Earth and the Moon, while in lunar orbit, and on the surface of the Moon. It will also use the data it collects to conduct onboard and ground-based navigation experiments using the collected information. These investigations are going to be based on the observation of the data that was collected by a custom development that was carried out by the company Qascom, and it was based on the Qascom QN400-Space GNSS receiver. The QN400's hardware construction as well as its software implementation are both modular in nature. A Radio Frequency (RF) front-end and a baseband processor that is created using Software Defined Radio (SDR) technologies are the two primary components that make up the receiver. PVT solutions, GNSS raw observables obtained by the real time operation, as well as snapshots of IF digital samples collected by the RF front-end at frequencies L1/E1 and L5/E5 for GPS and Galileo can all be provided by the receiver. Additionally, the receiver is able to provide snapshots of GNSS raw observables obtained in real time. These data will be the input for the various scientific investigations, which will then require the development of appropriate analysis tools in order to serve as the core of the ground segment while the mission is being carried out.

The science team of NASA and ASI, which is supported by a research team at Politecnico di Torino, is currently working on planning the data acquisitions that will take place during the time windows that are dedicated to the LuGRE payload during the checkout, transit, and surface mission phases.

The purpose of this thesis is to investigate the different types of processing that can be performed on a snapshot that has been recorded by the Qascom receiver over a specific amount of time. This can be helpful when planning the time windows that will be dedicated to the collection of snapshots as well as designing the duration of those time windows. In order to accomplish this goal, the snapshots were simulated by both our team and Qascom by accurately modeling the space environment. This is an essential step, as this type of analysis has never been conducted and there is no signal available at these distances. The tracking stage, which is more critical than the acquisition stage, is the primary focus of the analysis. The goal is to come up with a snapshot duration that enables at least one tracking lock condition to be reached. The collection of snapshots enables multiple functionalities, such as the potential to carry out additional advanced signal processing, to cross-validate with the results of the processing that occurs on-board, and to put risk mitigation into effect. In addition, the capability of tracking at least one signal guarantees an additional estimation of the C/N0 that can be cross-checked with the estimation provided by the real time receiver. Considering that the on-board estimation of the C/N0 is based on the acquisition stage, which is typically less precise than that which is based on the tracking, this can be an extremely helpful feature. However, the value of the snapshot duration is constrained by the limitations of data storage and transmission, which puts a stringent boundary on the value. As a result, the examination of this thesis assumes an extremely preeminent position.

Table of Contents

List of Figures

List of Tables

Acronyms

ACF Auto-Correlation function

ADC Analogue-to-Digital Converter

ASI Agenzia Spaziale Italiana

BDS BeiDou Navigation Satellite System

BOC Binary Offset Carrier

C/A Coarse/Acquisition (code)

C/N0 Carrier-to-noise ratio

CAF Cross-Ambiguity Function

CCF Cross-Correlation Function

CDMA Code Division Multiple Access

CS Control Segment

DFT Discrete Fourier Transform

DLL Delay Lock Loop

DoD Department of Defence

DSN Deep Space Network

DSP Digital Signal Processing

DSSS Direct-Sequence Spread Spectrum

EKF Extended Kalman Filter

ESA European Space Agency

EU European Union

Estrack European Space Tracking

FDMA Frequency Division Multiple Access

FFT Fast Fourier Transform

FLL Frequency Lock Loop

GDOP Geometric Dilution of Precision

GEO Geostationary-Earth Orbit

GLONASS Globalnaya Navigazionnaya Sputnikovaya Sistema

GNSS Global Navigation Satellite System

GPS Global Positioning System

IEEE Institute of Electrical and Electronics Engineers

IF Intermediate Frequency

IFFT Inverse Fast Fourier Transform

INS Inertial Navigation System

ISECF International Space Exploration Coordination Group

LEO Low Earth Orbit

LoS Line-of-sight

LS Least-Squares

LuGRE Lunar GNSS Receiver Experiment

MMS Magnetospheric Multiscale

MEO Medium Earth Orbit

ML Maximum Likelihood

MSO Moon Surface Orbit

MTO Moon Transfer Orbit

NASA National Aeronautics and Space Administration

NEIL Navigation Early Investigation on Lunar surface

NavSAS Navigation Signal Analysis and Simulation

OF Orbital Filter

p.d.f. Probability Density Function

PLL Phase Lock Loop

PNT Positioning, Navigation and Timing

POD Precise Orbit Determination

PRN Pseudo Random Noise

PVT Position, Velocity, Timing

RE Radius Earth

RF Radio Frequency

SDR Software-Defined Radio

SIS Signal-in-Space

SNR Signal-to-noise ratio

SS Search Space

SSV Space Service Volume

TTFF Time To First Fix

TTL Time to Lock

U.S. United States

VLBI Very Large Baseline Interferometry

WGN White Gaussian Noise

WLS Weighted-Least-Squares

Chapter 1

Introduction on GNSS

A Global Navigation Satellite System (GNSS) is defined as a group of satellites appropriately placed to provide positioning, timing, and navigation data from space to GNSS receivers. Thanks to this transmitted information, the receivers are able to determine their position, velocity and time. A GNSS satellite is designed to guarantee widespread global coverage on the Earth surface following four criteria:

- Accuracy: the degree of conformance of that position with the true position, velocity and/or time of the receiver;
- Integrity: the measure of the trust that can be placed in the correctness of the information supplied by a navigation system;
- Continuity: is the ability of system to perform its function without interruption during the intended operation;
- Availability: the percentage of time that the services of the system are usable by the navigator [1].

Furthermore, a navigation system is composed of three segments: the Space segment, the Control segment and the User segment.
The Space segment is the constellation of satellites from which users receive the signal to make ranging measurement.
The Control segment (CS) is responsible for monitoring the satellites in order to maintain their proper functioning.
The User segment consists on the user equipment allowing you to perform signal reception, that is the GNSS receiver task.
The first GNSS system implemented is the Global Positioning System (GPS). GPS was originally developed from the United States (U.S.) for military purposes, but is now provided as a public service for people all over the world by the U.S. government. The GPS constellation was, in the first instance, composed by 24 satellites flying in medium Earth

orbit (MEO) at an altitude of approximately 20,200 km meaning that each spacecraft gyrates the Earth approximately twice a day. The satellites are disposed in 24-slot arrangement so that the user can have at least four satellites in Line-of-sight (LOS).
Nowadays, the numbers of operational spacecrafts grows to 31 to ensure better performances of the system [2].
Following the GPS, Soviet Union developed the Globalnaya Navigazionnaya Sputnikovaya Sistema (GLONASS) constellation. GLONASS system consists in 24 number of nominal satellites with a period of revolution equal to 11 hours and 15 minutes, slightly lower than that of GPS. The number of orbital planes is now reduced to three against the six of GPS and even the Orbit inclination changes to 65 deg (55 deg for GPS). Even if the number are different, each GNSS system is designed to ensure the visibility of at least four satellites [3].
The most recent GNSS system is GALILEO, developed by a cooperation between the European Union (EU) and the European Space Agency (ESA). It is composed of 30 spacecrafts with an orbital altitude of 23,222 km and a period of revolution of 14 hours 22 minutes. The inclination is similar to that of GPS 56 degrees [4].
Even China has its own GNSS system called BeiDou Navigation Satellite System (BDS). Besides the 27 MEO satellites, the BDS constellation includes 5 Geostationary-Earth Orbit (GEO) satellites and 3 Inclined Geosynchronous Orbit, with a total of 35 number of operational satellites [5].

1.1 Determining the Distance using Radio Wave

The determination of the position and speed of the receiver is performed through an electromagnetic signal. To be more specific, the estimated parameters of the radio wave is employed and converted into estimated distances given that the position of the satellites is known. However, one satellites identifies a distance that is not a position but a line of positions. In the case of GNSS the line of position is sphere of radius R

$$R = c(T_{RX} - T_{TX}) = c\tau \tag{1}$$

where c is the speed of light, and τ is the delay defined as the difference between the time at which the signal was transmitted from the satellite and the time of arrival of the user. Position can be the obtained by means of intersection of different lines of position (spheres) which translates into a system equations to be solved. This process is referred to Trilateration and two examples of this are showed in Figure 1.1.

The GNSS system is a one way signal measurement meaning that all the transmitters must be synchronized. The synchronization process is done through an atomic clock aboard each satellite, but for sake of costly this cannot be implemented in the user segment. Consequently, the receiver and the transmitter are not synchronized introducing a bias during the computation of (1). The equation changes to

$$\rho = c\tau + c\delta t_u = c\tau + b_u \tag{2}$$

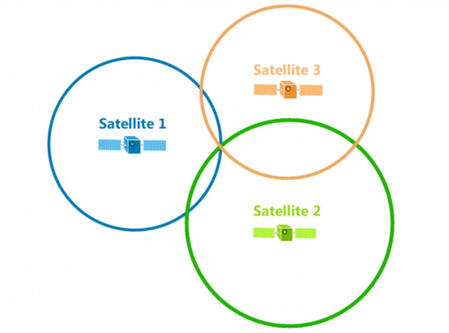

(a) 2D system

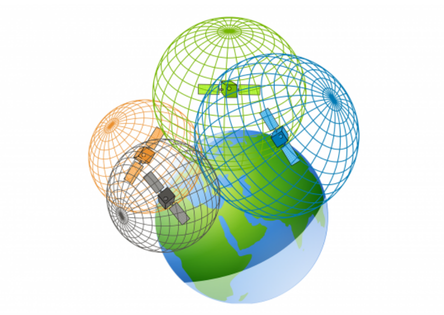

(b) 3D system

Figure 1.1: Examples of Trilateration. Source:[6].

where ρ is now called pseudorange since it is not a real geometrical distance anymore. As we can notice from (2), the user clock bias is multiplied by the speed of light, which results in a huge amplification factor that leads to a significant error on the distance even if the clock bias is relatively small. Furthermore, the clock bias is a further unknowns of the system that is added to the three coordinates of the position $P(X_u, Y_u, Z_u)$, with a total of 4 unknowns. Therefore, in order to solve the system a number of pseudorange equations equal to four is needed which translates into four satellites in LoS for the user. This is the reason why during the previously presentation of the different GNSS system, each of them ensures to have at least four satellites in visibility. Theoretically, four number of satellites are enough to find the position, but in practice a larger number of them can be needed to improve the performance of the system.

1.1.1 Positioning error and GDOP

In order to understand why having a larger number of satellites in LoS is beneficial, a discussion on the positioning error should be done. The standard deviation of the positioning error can be computed as

$$\sigma_x = GDOP \cdot \sigma_{UERE} \tag{3}$$

where Geometric Dilution of Precision (GDOP) is a number strictly greater than 1, describing the impact of the geometry on the solution. The GDOP is the ratio of the location fix's accuracy to the statistical accuracy of the ranging measurements. Consequently, the general accuracy of a position estimate can be stated as the product of the GDOP at a location and the root mean square error of the ranging errors from the mobile device to the measurement nodes. If the placement and quantity of base stations in the target coverage region are not carefully designed for a terrestrial system, the GDOP effect can become the limiting factor for system performance. The GDOP concept was initially intended

to explain the performance of terrestrial navigation systems, but it was later applied to evaluate the geometric effect of satellite configurations on GNSS precision. When satellites' angular positions are close in the sky, the GDOP value is large, resulting in poor positioning performance [7].
Therefore, the GDOP says to us that the impact of the pseudorange error on the final estimated position depends on the satellites' geometry. Increasing the number of satellites in LoS, improves the displacement of them meaning that the GDOP is reduced. Since the GDOP is an amplification factor of the positioning error (3), a GDOP reduction results in a better estimation of the final position. Additional information can be found on [8].
The σ_{UERE} takes into account all the type of errors of the system such as propagation errors, ephemeris errors, but in the condition in which all the biases were previously compensated. To go into details, UERE stands for user user equivalent range errors and its standard deviation is computed, as anticipated before, as the root mean square error of the ranging errors affecting the user position.

1.2 Characteristics of GNSS Signals

Signal-in-Space (SIS) is the name of the signal that is continuously transmitted by the GNSS satellites. This SIS is composed by three main components: Carrier, Ranging code and Navigation data as depicted by Figure 1.2.

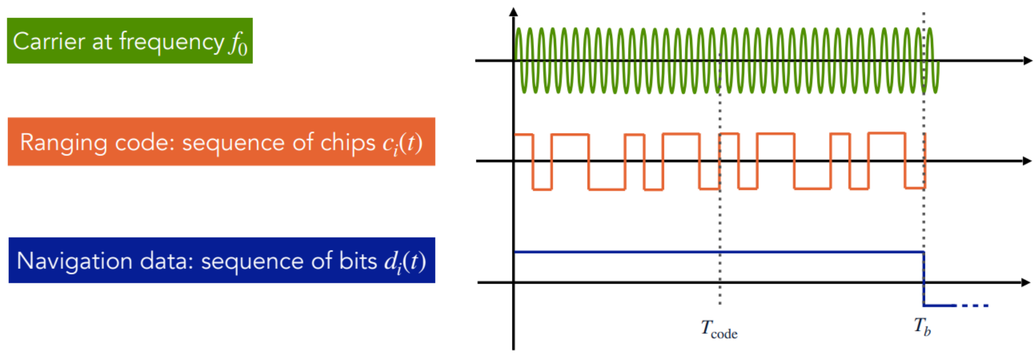

Figure 1.2: Main components of GPS L1 C/A signal

The carrier is a Radio frequency sinusoidal signal at a given frequency. Figure 1.3 shows the GNSS frequency bands. We can notice that the GNSS signals are transmitted using frequencies from 1 to 2 GHz. This range of frequencies is denoted as L-band by the Institute of Electrical and Electronics Engineers (IEEE).

The L-band presents some benefits with respect other frequency bands, in terms of delays and robustness with respect to attenuation caused by Earth's atmosphere and by precipitations.

The ranging codes (second component mentioned) are sequences of zeros and ones with great mathematical properties in terms of orthogonality, which allows you to overlap the signal transmission in time and frequency without suffering interference. They are called Pseudo-Random Noise (PRN) sequences or PRN codes. The PRN codes are also used to estimate the pseudorange by the receiver, or in other words to estimate the propagation time of the signal.
The majority of the GNSS system exploits the ranging codes to perform Code-Division-Multiplexing access (CDMA) technique. CDMA ensures the satellite identification without ambiguity even if more satellites are broadcasting at the same time and at the same frequency. Employing CDMA means using Direct Sequence Spread Spectrum (DSSS) concerning the modulation. DSSS consists in enlarging the bandwidth of the signal by means of a multiplication of the latter by a chip sequence (in our case the ranging code). Spreading the spectrum presents several advantages in terms of security and robustness. Each satellite, then each transmitter employs a different code as chip sequence. The last component is the navigation data, a binary-coded message providing information on the satellite ephemeris (Keplerian elements or satellite position and velocity), clock bias parameters, almanac (with a reduced accuracy ephemeris data set), satellite health status, and other complementary information [9].

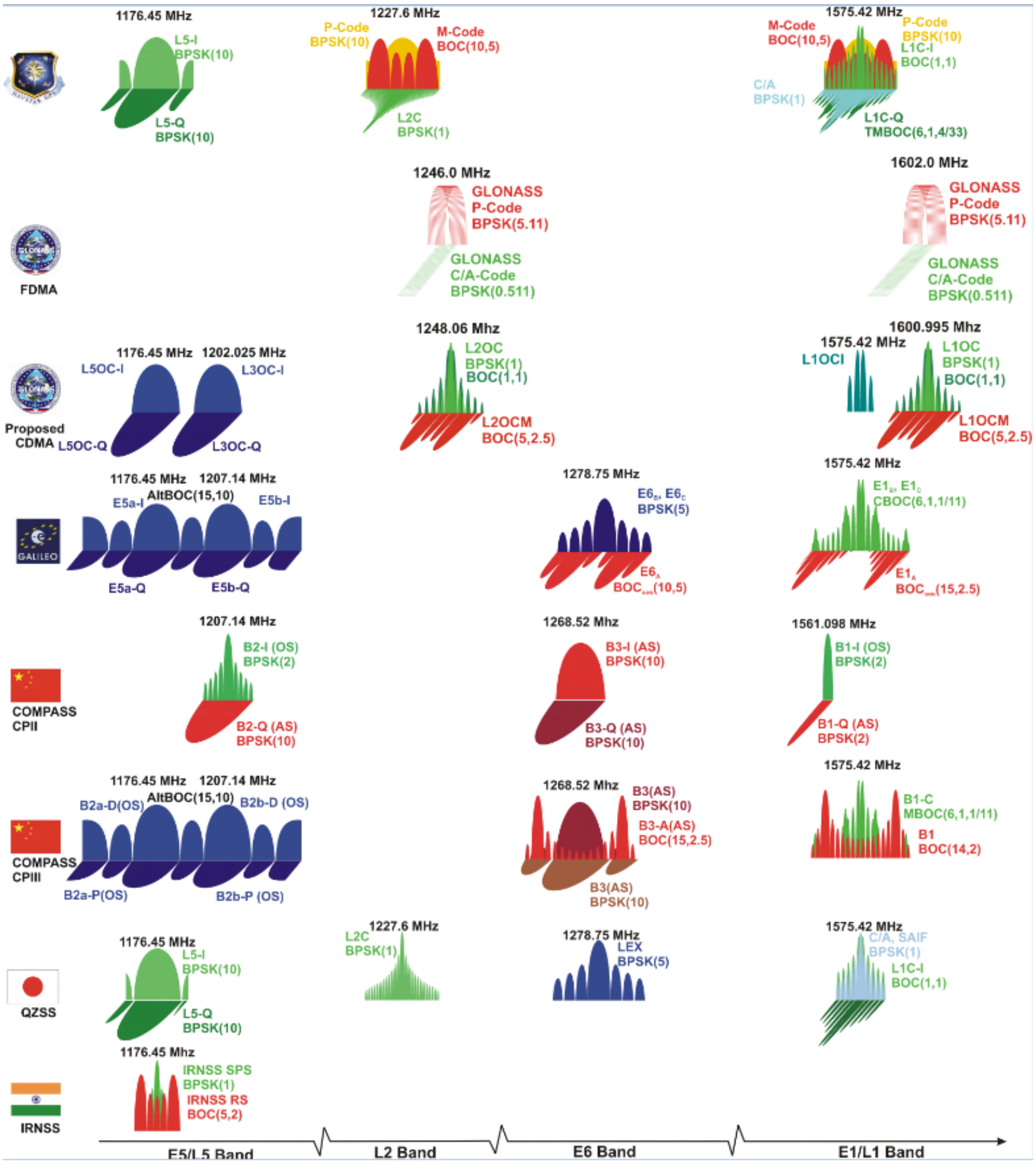

Figure 1.3: GNSS Frequency bands. Taken from [9].

1.2.1 GPS signal structure

Concerning GPS, the RF sinusoidal signal with a carrier frequency of $f_{L1} = 1575.42\ MHz = 154 \cdot 10.23\ MHz$ and $f_{L2} = 1227.60\,MHz = 120 \cdot 10.23\ MHz$, derived as multiple of 10.23 MHz to keep synchronized the satellites. Two ranging codes are employed:
Coarse/Acquisition (C/A) code and Precision (P) (Y if encrypted) code, that are both combined with a binary navigation data. GPS satellites broadcast two signals on frequency L1 one for the standard positioning service of civil users and one reserved for Department of Defence (DoD)-authorized users only. Just a unique signal for DoD-authorized users is transmitted on frequency L2. The C/A codes are characterized by a short duration that ensure a fast, but less precise acquisition of the signal. The code length is p = 1023 chips with a total duration of the code equal 1 ms, which results in a chip duration around $1\mu s$. Differently, the P code is extremely long reaching a code duration of 1 week. The shorter chip time translates into a great precision in range measurements even if the processing time grows.
Summarizing, the SIS transmitted by the k-th GNSS satellite has a form of

$$\begin{aligned} s_{RF}^{(k)}(t) = &\sqrt{2P_C} \cdot x^{(k)}(t)d^{(k)}(t)cos(2\pi f_{L1}t + \theta_{L1}) \\ &+\sqrt{2P_{Y1}} \cdot y^{(k)}(t)d^{(k)}(t)sin(2\pi f_{L1}t + \theta_{L1}) \\ &+\sqrt{2P_{Y2}} \cdot y^{(k)}(t)d^{(k)}(t)sin(2\pi f_{L2}t + \theta_{L2}) \end{aligned} \tag{4}$$

where P_C, P_{Y1} and P_{Y2} are the signal powers respectively for C/A-code on L1, P(Y)-codes on L1 and L2, while x(t) and y(t) correspond to the C/A code and the P(Y) code of the satellite k. Moreover, d(t) is the navigation bit stream of the k-th satellite. Since a cosine is present in the C/A code, it is the quadrature component of the signal, while the P-code is the in-phase one given the presence of a sine function.

1.2.2 Galileo and BOC signals

Galileo system applies a further modulation referred to split spectrum or Binary Offset Carrier (BOC) modulation in order to transmit on the same carrier of other GNSS systems reducing the mutual interference. BOC consists in introducing a frequency shift, modulating the signal with a sub-carrier which results in a shift of the signal spectrum with respect the main carrier. BOC modulation is characterized by two parameters: n that is the sub-carrier frequency in multiples of 1.023 MHz and m that is the chip rate in multiples of 1.023 Mcps, the notation used is BOC(n,m). Figure 1.4 shows the power spectrum of GPS-BPSK, BOC(1,1) and BOC(10,5). We can notice that the width on the main lobe depends on the code rate (m) given that the BOC(10,5) presents a larger lobes than other, while the shift depends on the sub-carrier frequency (n).

Moreover, Galileo satellites transmit permanently three independent CDMA signals, named E1, E5 and E6 respectively with a carrier of 1575.420 MHz, 1191.795 MHz and 1278.750 MHz [10]. Each signal is the results of applying a five multiplexing scheme to

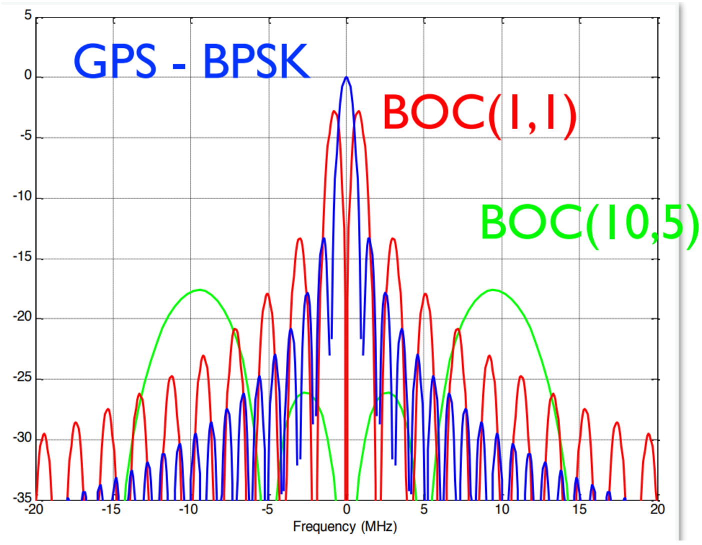

Figure 1.4: Comparison of the Power spectrum for different modulation.

combine a set of components, generated combining more channels. The whole transmitted Galileo E1 signal consists of the multiplexing of three channels: E1b is the data channel, E1c is the pilot channel and E1p is a part of the data channel with restricted access. (Figure 1.5)
Two Navigation Signals are transmitted in the four channels of E5-band signal, while two Navigation Signals transmitted in the three channels of E6-band signal named E6c (commercial access signal) and E6P (restricted access signal).

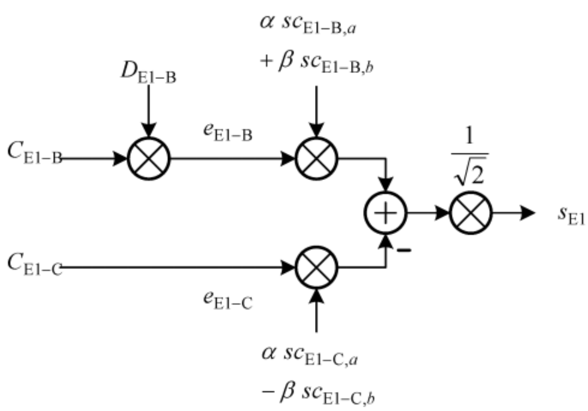

Figure 1.5: Modulation Scheme for the Galileo E1 Signal. Source:[10].

1.3 Typical GNSS receiver architecture

The main task of the GNSS receiver is to measure the propagation time of the signal with high precision. The operations that a navigation receiver executes are:

- Receive, amplify and filter GNSS signals transmitted by satellites and apply Analog-To-Digital conversion;
- Separate the different channels and generate local codes replica to demodulate the signal;
- Extract GNSS signal code phase for pseudorange measurement and carrier phase for carrier phase measurement;
- Demodulate the navigation message and solve the PVT equations.

The mentioned operations can be grouped in five main blocks composing a typical GNSS receiver architecture that are:

- Antenna and front-end stage;
- Acquisition stage;
- Tracking (code and phase) stage;
- Data Demodulation;
- Position estimation;

Acquisition and Tracking belongs to the Digital Signal Processing (DSP) part and works on different and independent channels simultaneously, one channel is dedicated for each satellite. For sake of explanation, only a single channel is analyzed in the presentation of the receiver stages. Acquisition is a preliminary but fundamental step, revealing which satellites are in LoS to start the processing of them. Subsequently, its output is given as input to the tracking stage, in which the delay and the Doppler is actually estimated. Once the pseudorange is computed, the PVT solution can be estimated. Acquisition and tracking must be run continuously in parallel, since the satellites are moving permanently, appearing and disappearing over time.

1.3.1 The front-end stage

The front-end stage is composed by three main components that are a filter, an amplifier and a mixer. An RF band-pass filter is employed to limits the bandwidth of the incoming signal before the down-conversion, preparing the input signal for the following sampling stage. Filtering ensures to reduce the noise, but it affects the signal shaping. After the

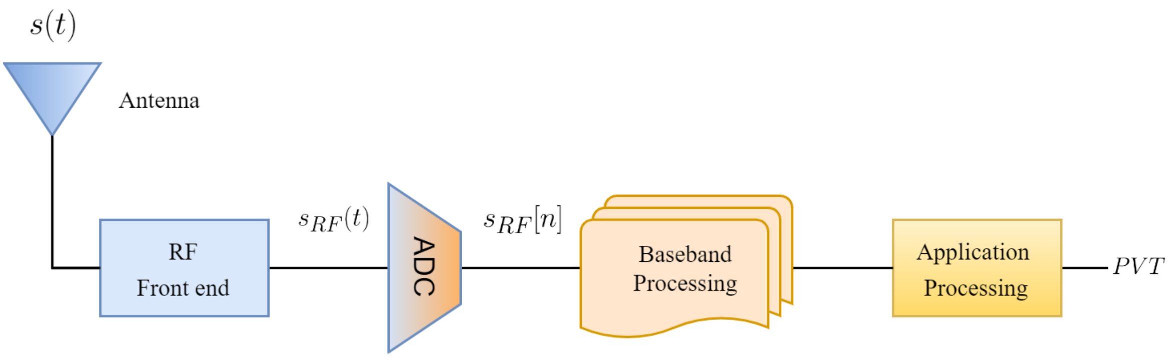

Figure 1.6: Generic GNSS Receiver Architecture.

filter, an amplifier is needed to increase the signal power of the received signal, taking into account that GNSS signals present very low power level. A mixer is then used to move the RF spectrum of the signal directly to base-band or, most commonly, to an Intermediate Frequency (IF) close to it. It is important to underline that the down-conversion does not compensate the shift but works according to the nominal carrier frequency meaning that the Doppler remains equal before and after the processing. Finally, Sampling and Quantization are applied to the signal, that is the analog to digital conversion by means of Analogue-to-Digital Converter (ADC). Hence, the signal is ready to be processed by DSP. The sampling frequency (f_s) depends on the bandwidth of the filter (B) that is the maximum frequency of the signal after the IF filtering following the Nyquist–Shannon sampling theorem

$$f_s = \frac{1}{T_s} \geq 2B \tag{5}$$

Carrier-to-noise ratio definition

Besides the sampling frequency, the power of the receiver signal depends on the bandwidth of filter. The bandwidth must be large enough to avoid filtering useful signal power. Therefore, the value of Signal-to-noise ratio (SNR) commonly defined as the ration between the signal power and the noise power depend on the front-end filter employed. Hence, in GNSS a quantity is introduced to describe the power-noise level independently from the architecture of the receiver. It is called Carrier-to-noise ratio (C/N0) and it is defined as the ration between the signal power evaluated on the entire signal bandwidth (C) and the noise power density (N0). The C/N0 is measured in dB-Hz and it can just be estimated by the receiver, cannot be directly computed. The link between the SNR and C/N0 is

$$\frac{C}{N_0} = SNR \cdot B \tag{6}$$

At the end, the signal at the output of the front-end stage is

$$\begin{aligned} s_{RF}^{(k)}[n] = \sqrt{2P_{RX}} \cdot \hat{x}^{(k)}(nT_S - \tau)d^{(k)}(nT_S - \tau) \\ b_c^{(k)}(nT_S - \tau)sin(2\pi(f_{IF} + f_d)nT_s + \theta) + w[n] \end{aligned} \tag{7}$$

where τ is the delay of the code replica with respect the signal, T_s is the sampling time, $\hat{x}$ is the filtered code, b_c is the filtered sub-carrier (presents only for Galileo signal), f_d is the Doppler shift and $w[n]$ is the noise component modelled as a White Gaussian Noise (WGN).

1.4 The Acquisition stage

The discrete-time output of the down-converted received signal is provided by the front-end stage as its final output (7). This signal is characterized by three unknowns that are the code delay τ, the Doppler frequency f_d and the phase θ. The information regarding the clock and range can be found in the code delay, while the information regarding the pseudorange rate can be found in the Doppler, and the phase is essential for having high precision. The stages of the receiver known as Acquisition and Tracking are the ones that are responsible for making estimates for the mentioned parameters. The task of acquisition is to provide an initial rough estimate of the delay and Doppler shift between the incoming code and the local replica, while the phase is not taken into account during this stage in the process. Before attempting to estimate the parameters, an operation known as Detection, which entails determining which satellites are located in Los, must be carried out as part of the initial processing. Estimating the functions of correlation is essential to the successful completion of these operations. As was stated earlier, the PRN codes, in point of fact, are distinguished by great mathematical proprieties in terms of orthogonality. When there is a correlation between the code and itself, we refer to this as an auto-correlation function (ACF), but when there is a correlation between two different codes, we refer to this as a cross-correlation function (CCF). The ACF of a PRN sequence is characterized by a peak in correspondence of the zero shift, and in all other cases, the value is extremely close to zero. As a result, this peak does not appear in the CCF function, and its absence means that it can be used to determine whether or not a satellite can be seen, as well as to calculate the Doppler shift and the delay of the signal that has been received. In practice, the GNSS receiver creates a local replica of the code and then experiments with various values of delay and carrier before carrying out the CCF between the local replica and the incoming signal. When a peak of correlation appears, indicating that the CCF is likely to be an ACF, then the satellites associated with that PRN are acquired. The Maximum Likelihood (ML) method of estimating the parameters is used in the process of performing the parameter estimation.

1.4.1 The Cross ambiguity function

The correlation function used by a GNSS receiver is a two-dimensional correlation with the delay and Doppler as independent variables. It allows the comparison between the incoming signal and a local replica in order to achieve the best estimation of the parameters. This function is called Cross-Ambiguity Function (CAF) and it is defined as

$$R(\bar{\tau}, \bar{f}_d) = \frac{1}{N} \sum_{n=0}^{N-1} s_{RF}[n] x(nT_S - \bar{\tau}) b_c(nT_S - \bar{\tau}) e^{j2\pi(f_{IF}+\bar{f}_d)nT_S} \tag{8}$$

where s_{RF} is the incoming signal, while the remaining factors constitute the local replica (the sub-carrier must be added in case of Galileo signal). $\bar{\tau}$ and $\bar{f}_d$ are the set of delay and Doppler values over which the function is evaluated. A complex exponential is taken into account (8) since the phase of the received signal in not estimated at this stage and the modulus square of CAF is considered during the computation $S(\bar{\tau}, \bar{f}_d) = \left|R(\bar{\tau}, \bar{f}_d)\right|^2$. As said before, this envelope is evaluated over a set of values $\bar{\tau}, \bar{f}_d$ defining a grid referred to the Search Space (SS). The points of the grid are called respectively delay and Doppler bins and they defines the size of the SS as $N_\tau \times N_D$ bins. The number of the delay bins N_τ depends on the sampling frequency $f_s = \frac{1}{T_s}$ and on the coherent integration time. The sampling frequency should be big enough to ensure a precise estimation of the acquisition parameters to make the tracking converge. The coherent integration time is defined as the time window in which the correlation function is evaluated $T_{coh} = NT_s$ and it is a multiple of the code period T_{code}. The number of delay values to be tested is then

$$N_\tau = \frac{T_{coh}}{T_s} = f_s T_{coh} \tag{9}$$

It is important to underline that what is actually estimated during the acquisition is not the delay but the code phase due to periodicity of the incoming code.
Regarding the Doppler resolution, it is a more critical value to be choose given that it is strictly related to the specific application of the receiver. The Doppler range to be searched depends on both the applications and some parameters such as the satellite motion, user motion and the user clock drift. However, the Doppler bin size depends on the integration time since a smaller value of integration time means a wider correlation function. Many GNSS receiver adopts an empirical rule ensuring the worst case loss to be less than 3dB, that is

$$\Delta f = \frac{2}{3T_{coh}} \tag{10}$$

An example of acquisition result is proposed in Figure 1.7. The plot displays a normalized 3D CAF obtained processing a Galileo E1c signal. In the x-axis are placed the values of the code delay [chips], while in the y-axis the values of the Doppler [Hz] and the z-axis represents the values of the correlation function normalized to its maximum value. We can observe that a clear peak emerges from the noise floor, exceeding distinctly the threshold represented by the horizontal red plane meaning that the acquisition of that satellite is accomplished successfully.

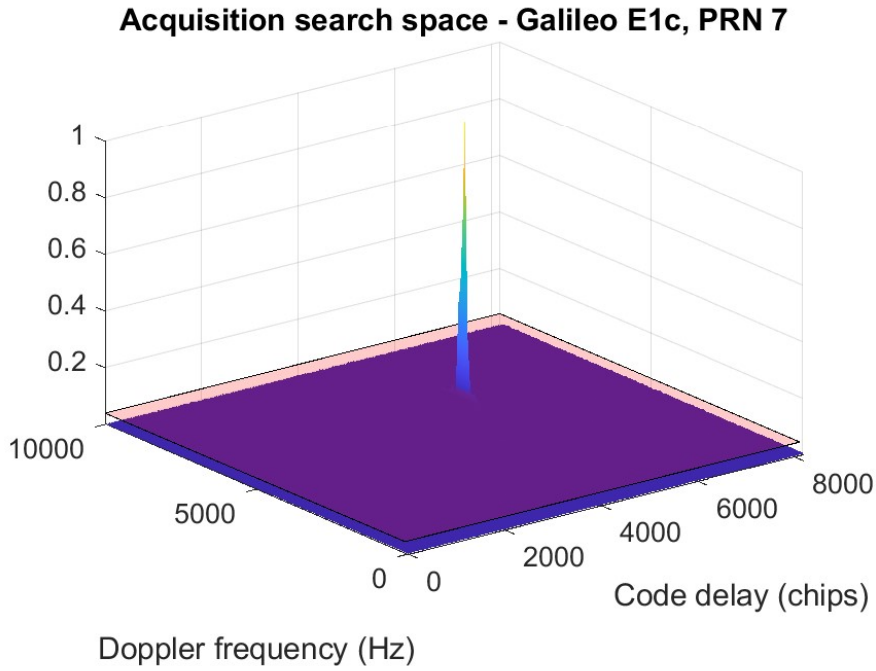

Figure 1.7: Example of CAF for a GAL E1c signal, PRN code 7

It is relevant to highlight that the Acquisition has a crucial impact on the Time To First Fix (TTFF), one of the key parameters of performance of a GNSS receiver. The TTFF is defined as the time needed to acquire the satellites and get the PVT solution. The acquisition is the major contribution affecting the TTFF, therefore it must be simpler and faster as possible. The larger is the size of the SS, the longer will be the execution time and the smaller will be the value of the TTFF of the receiver. Therefore, one way to make the receiver faster is to reduce the SS of the acquisition. However, a reduction of the SS size led to a lower probability to acquire the satellites. A trade-off arises between the ability to acquire the satellite and the ability to do this quickly. In practice, a possible solution could be to retrieve some external information such as Clock, almanac data or last known location. In this case we talk about a warm or hot start-up of the receiver since the size of the SS is reduced by means of this information. Differently, if no external information is available to the receiver, the entire search space must be evaluated and we talk about Cold start-up.
Furthermore, another factor contributing on the acquisition processing time is the complexity of the strategy employed to compute the CAF. The CAF can be evaluated using a serial or a parallel search. The serial search presents an easy implementation in which a

single value of the correlation function is obtained at each trial. However, it identifies the parameters by exhaustive search meaning that the correlation is evaluated for each single point of the grid at time so that the time required is proportional to the number of bins to explore. Summarizing the serial search is easy but time consuming. The parallel search is performed in one of the two domains by means of the FFT operations and reduces the complexity of the serial acquisition systems. It is the most used architecture since it allows to reduce the TTFF and it is adopted also in this thesis work. Parallel search can be done on both time and frequency domain. Figure 1.8 shows a block scheme of the strategy using parallel acquisition in time domain (the one employed for this thesis).

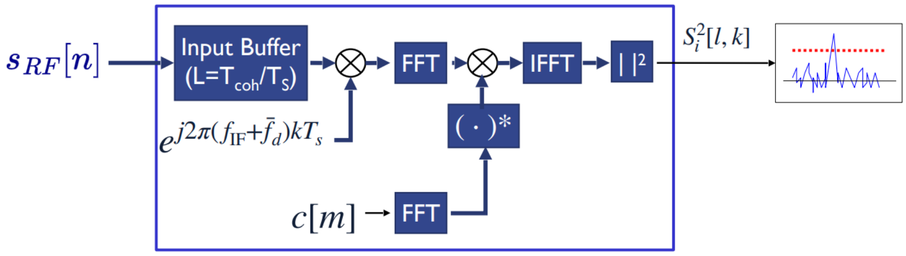

Figure 1.8: Block diagram - Parallel acquisition in time domain

1.5 The Tracking stage

Acquisition provides a fast and rough estimate of the delay $\hat{\tau}^{(a)}$ and Doppler $\hat{f}_d^{(a)}$ parameters. The latter are employed to initialize the tracking stage which has the task to refine and track continuously them. The refining process is performed by following an iterative approach in which the fresh values of Doppler and delay are supplied to the wiping blocks, which progressively improve the quality of the estimate and the synchronization of the signal. Figure 1.9 illustrates the block diagram of the mentioned process, in which four main blocks composes the tracking and they can be combined in different ways depending on the receiver implementation.

The first blocks of the branches are wiping blocks respectively named code wipe off and carrier wipe off. In fact, a precise estimate of the carrier frequency and the phase cannot be obtained if the code is not removed from the signal and similarly a precise estimation of the delay cannot be done until the residual modulation is present. The more precise are the values of the parameters as input, the more accurate will be the outputs. The presence of the double loop in the tracking architecture makes very hard to study its behavior and it does not exist a closed mathematically form to describe the convergence of the system. The tracking stage converges to the best solution of the parameters only if the initialization values provided by the acquisition are precise enough. If the tracking

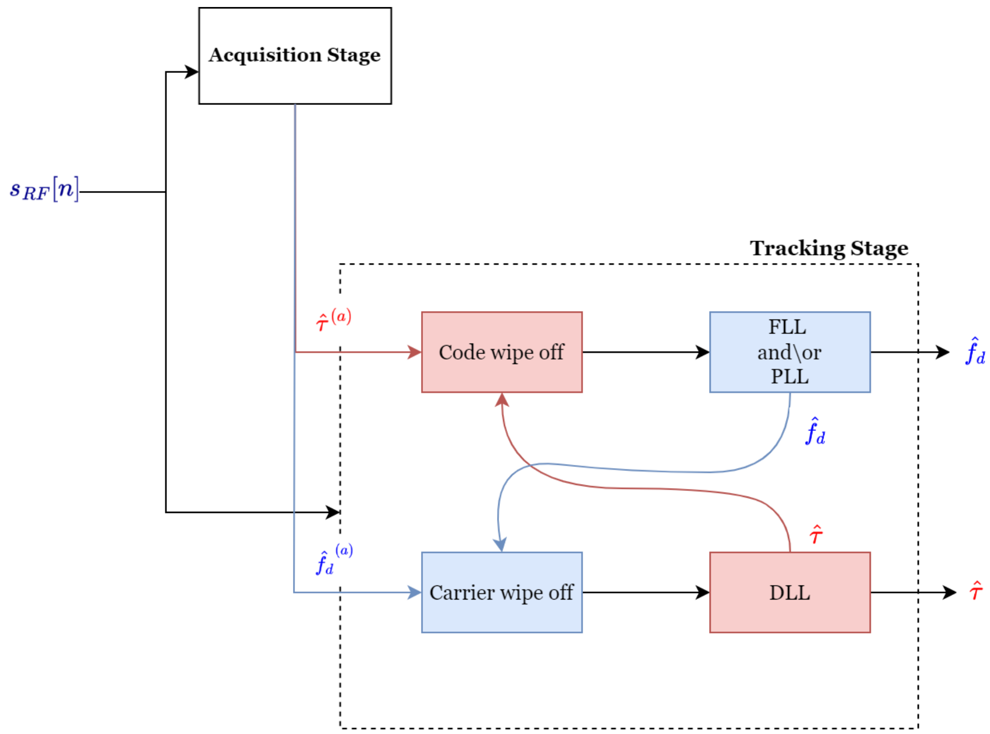

Figure 1.9: Block diagram - Tracking stage

converges to a solution, it is said to be locked meaning that a stable solution of the double loop is found. The tracking estimates are then employed to construct the pseudorange. Therefore, the tracking stage can be considered the core part of the GNSS receiver given that the quality of the pseudorange measurement is strictly related to the quality of the tracking. A bias in the tracking loop directly translates in a bias in the pseudorange measurement.

1.5.1 Carrier tracking loop

The first branch of the tracking is represented by the chain code wipe off and carrier tracking. As mentioned before, before tracking the carrier it is needed to remove the code from the signal. The code wipe off consists in multiplying the incoming signal with local code delayed of $\hat{\tau}$

$$s[n] = c(nT_s - \hat{\tau}) \cdot s_{RF}[n] \tag{11}$$

the remaining signal s[n] is a continuous sinusoidal wave. If the delay is not perfectly estimated, a residual modulation compares in the signal which results in spikes on the wave of which the duration depends on the value of the code misalignment. Anyway, this high frequency disturbance does not represent a big issue since it is directly filtered by the carrier loop which acts as a narrow-band filter.

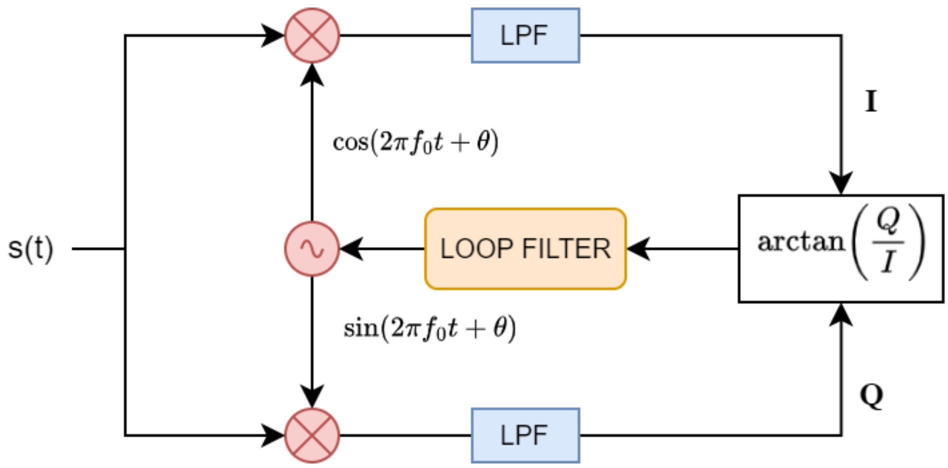

Figure 1.10: Block diagram - Costas loop implementation of the PLL

The carrier tracking loop is a feedback loop able to finely estimate the frequency and the phase of a noisy sinusoidal waveform and to track the frequency changes while the satellite is moving. The carrier tracking loop is defined by the carrier loop discriminators that can be a Phase lock loop (PLL) or a Frequency-locked loop (FLL). FLL tracks the Doppler frequency completely ignoring the carrier phase. The latter is more robust against dynamic stress, but it is less accurate than PLL. To take advantage of both, generally an FLL-assisted PLL is used in a GNSS receiver. In fact, it can be demonstrated that by using both FLL and PLL is possible to achieve the convergence in a shorter time than using the PLL only. This because FLL provides a more accurate value of frequency allowing the PLL to work on a narrow band which results in a shorter transient time. Figure 1.10 shows an example of PLL implementation named Costas loop implementation. The presented discriminator computes the difference between the phase of the incoming signal and the locally generated signal. During this work thesis a two-quadrant Costas PLL discriminator is employed, which outputs the phase error as

$$\delta\varphi_k = \arctan\left(\frac{Q_{k,d/p}}{I_{k,d/p}}\right) \tag{12}$$

where $\delta\varphi_k$ is the estimated carrier phase error over the integration time [35].

1.5.2 Code tracking loop

Before fine estimating the delay, the modulation must be removed. The carrier wipe off is performed by means of the heterodyne method consisting in multiplying the signal by a sinusoidal signal generated by a local oscillator, in principle perfectly locked to the incoming carrier thanks to the estimate of the Doppler shift and the carrier phase. The result of this operation is a signal translated perfectly in base-band and from which information on the delay can be retrieved. The code or delay tracking loop in then performed by means of a block called Delay lock loop (DLL). The delay information is contained in the correlation peak, but differently from acquisition searching the maximum is not employed in this stage. In fact, the DLL works by means of two correlators and two local replicas of the code. The local replicas generated are the early code (13), an early version of the incoming code, the late code (14), a delayed version of the incoming code and the prompt code (15), a version of the code aligned with the incoming one.

$$c_E[n] = c(nT_s - (\hat{\tau} + \frac{\Delta}{2})) \tag{13}$$

$$c_L[n] = c(nT_s - (\hat{\tau} - \frac{\Delta}{2})) \tag{14}$$

$$c_P[n] = c(nT_s - \hat{\tau}) \tag{15}$$

The spacing between the early and the late replicas is indicated with Δ. The DLL works in an iterative manner and at each step the delay is adjusted updating of $\bar{d_\tau}$ the initial estimation obtained during the acquisition phase. However, a strategy insensitive to the absolute peak value must be adopted. For this reason, a Discrimination function or discriminator is introduced, named S-curve and defined as difference between the Early and the Late correlators (Early minus Late). (16)

$$S(\epsilon_\tau) = R_c(\epsilon_\tau + \Delta/2) - R_c(\epsilon_\tau + \Delta/2) \tag{16}$$

The S-curve is function of ϵ_τ defined as the difference between the actual and the estimated delay $\tau - \hat{\tau}$. The mentioned discriminator constitutes a coherent DLL under the hypothesis that both the carrier frequency and carrier phase are estimated and removed by the PLL. Other types of non-coherent discrimination function exist such as the Early minus late normalized or the early minus late power normalized, making DLL more robust but still with a residual carrier phase.

Figure 1.11 shows the plot the plot of the Early minus Late discriminator and the Early and Late correlation functions for a spacing equal to 1 chip. We can notice that discrimination function is not ambiguous with respect to early-late misalignment of the codes. The DLL continuously corrects the delay on the basis of the input received by discriminator. When the zero of the S-curve is reached we are perfectly aligned with the incoming signal given that the prompt code is as distant from the early code as it is from the late one.

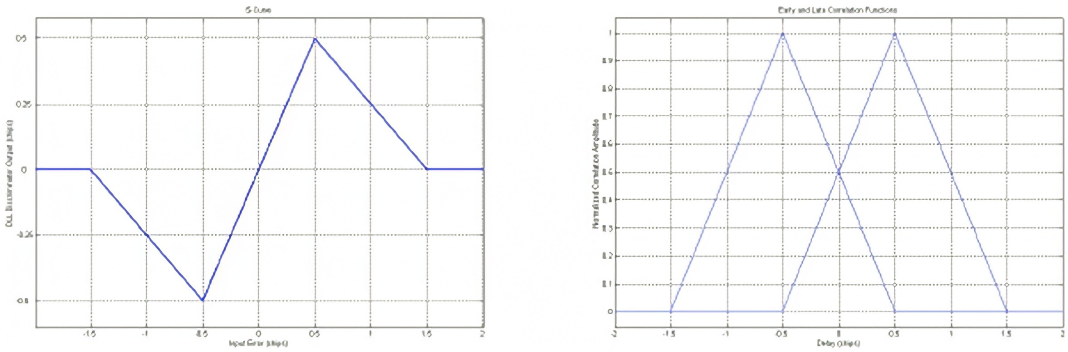

Figure 1.11: GPS Early and Late correlation functions (right) and S-curve: E-L (left). Source:[11].

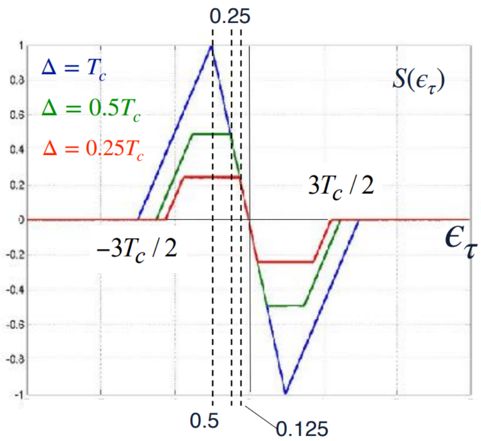

Figure 1.12: GPS E-L S-curve for different values of spacing.

Regarding the error component, the variance of the noise at the input of the DLL, if the noise is an Additive White Gaussian Noise (AWGN) can be computed as

$$\sigma_N^2 = \frac{\sigma_w^2 2\Delta}{P_R L T_c} \tag{17}$$

where the spacing appears at the numerator. Consequently, the variance of the noise at the input of the DLL is directly proportional to the early-late spacing meaning that a spacing reduction translates in a reduction of the effect of the thermal noise.
Figure 1.12 shows the GPS C/A E-L discrimination functions for different value of spacing: one code period, half of the code period and quarter of the code period. We can notice that the effect of reducing the spacing of a DLL makes the peak of the correlator smoothed with

a consequent reduction of the linear zone. The proposed fact presents another advantage of reducing the spacing. In fact, a narrow correlator is more robust against multipath effect on the pseudorange bias and then reducing the E-L spacing, makes the system more insensitive to the multipath effect.
However, even if the trend is having a narrow correlator, this also requires increasing the front-end bandwidth, which increases the vulnerability to in-band RF interference.

1.5.3 Tracking lock declaration

The dominant sources of phase error in a GNSS receiver PLL is the phase jitter. The phase jitter or tracking jitter is defined as the root sum square of every source of the uncorrelated phase error, such as thermal noise and oscillator noise [35]. The jitter is estimated by computing the standard deviation of the carrier phase tracking error defined in (12) and it can be used to compare different tracking outcomes. Furthermore, the standard deviation of the pseudorange error is proportional to the tracking jitter, thus the tracking jitter value describes the quality of the PVT computation as well. Frequently, the thermal noise of the PLL is considered the only source of carrier tracking error, since the other potential sources of PLL jitter are transient or negligible. The carrier thermal noise error standard deviation is strictly dependent on the carrier–to-noise power ratio, the noise bandwidth, and the integration time. The carrier-to-noise power ratio, C/N0, is an important factor in many GNSS receiver performance measures [25].
On the basis of error information, tracking convergence can be defined. In other words, if the tracking error is less than a specific limit, then the system will converge. When the convergence of the double loop is achieved, the tracking is said to be locked, indicating that the satellite's parameters are accurately estimated and tracked by the system. However, due to the presence of the double loop, the tracking architecture is complex and a closed form to mathematically describing the convergence of the system does not exist. As a result, the lock declaration is a challenging task and it cannot uniquely defined in a standard way.
Some indicators can be used to accomplish the presented task. One of these is named Phase Lock Indicator (PLI). The Phase Lock Indicator or Tracking Lock Indicator is computed by means of the prompt IQ correlator outputs of the carrier tracking algorithm

$$PLI_k = \frac{I^2_{k,d/p} - Q^2_{k,d/p}}{I^2_{k,d/p} + Q^2_{k,d/p}} \approx cos(2\Delta\varphi_k) \tag{18}$$

where $\Delta\varphi$ is the Phase Error already presented in (12).
The phase lock indicator concept is the following: if the loop is in phase lock, then I correlator will be maximum and Q correlator will be minimum. Figure 1.13 depicts the output of the in-phase and quadrature components of the prompt correlator. When tracking the signal correctly, the prompt vector should be, ideally, in the in-phase axis, with no quadrature component [12]. In this ideal situation the value of the PLI converges to

1. The more the PLI is near to the ideal value, then the lower will be the phase error at the output of the PLL. It is important to note that the PLI and the phase error concept are strictly linked with the phase jitter. As the phase jitter increases in the loop due to noise, dynamic stress, and so forth, the phase of the envelope jitters around the I-axis. Eventually, the jitter will reach a level where a cycle will be slipped or complete loss of phase lock occurs [25].
In practice, to implement a phase lock detector, a threshold is taken into account. Setting a threshold on the PLI value means fixing a value on the phase error to be tolerate. The higher the value of the threshold, the lower the phase error permitted, and then the lock declaration will be more confident and reliable. However, having a high threshold means also increase the probability to not declare a lock when this happens, especially for low value of C/N0. If a sample has a tracking lock indicator less than the threshold, then it is indicated as loss of tracking points [35].
Different algorithms can be employed to declare the lock based on the loss of tracking points. To give an example, the simplest one is the decision logic based on thresholding of the PLI value. When the PLI exceeds the value of the threshold for the first time, the first lock is achieved. On the contrary, if the PLI value goes below the threshold, the tracking is lost. The phase error threshold should be decided specifically depending on the environment and on the receiver features.
However, the mentioned decision logic does not work properly in case of low value of C/N0, since the threshold cannot properly set. In fact, to have a robust and reliable declaration a threshold near to 1 as possible must be choose, but as anticipated before, the risk is having an higher probability of missed detection. Conversely, reducing the value of the threshold means reducing the probability to miss a lock but it increases the probability of false alarm, that occurs when the lock is declared but the tracking does not actual converge. As a result, If we fix only a value of threshold in case of low C/N0, we cannot get a low probability of false alarm and a low probability of missed detection at the same time. In this case, more robust algorithm can be adopted, allowing to reduce the false lock declaration probability. An example of this is presented in [25]. It consists on employing two phase lock indicator, one optimistic and one pessimistic. The optimistic phase lock indicator makes decision quickly and changes its decision slowly but is less reliable. Conversely, the pessimistic lock indicator is more reliable because it is slower to decide and faster to change its mind. Figure 1.14 shows the block diagram of the presented algorithm. During the thesis a different approach will be proposed. It consists in using more consecutive values of the PLI over the threshold to make the decision logic more robust. In other words, besides the threshold a counter is considered. During the tracking loop, if the sample has a PLI over the threshold, the counter is decremented, while if the opposite situation the counter is reset to its initial value. If during the loop the counter goes to zero, the lock is declared. The starting value of the counter as well as the threshold should be set depending on the specific situation of the environment and the receiver.

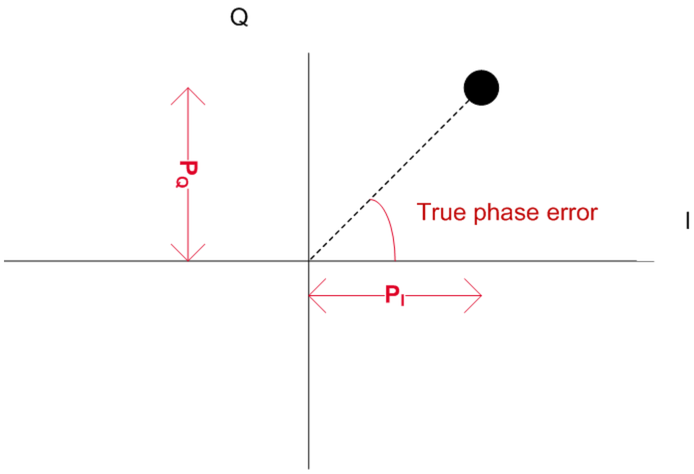

Figure 1.13: Representation of the Prompt Correlator output. Source:[12].

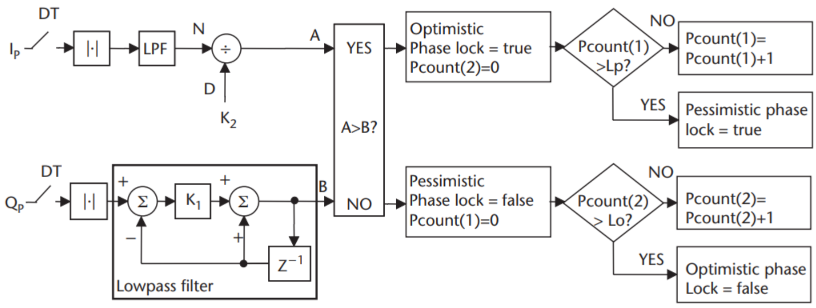

Figure 1.14: Basic phase lock detector with optimistic and pessimistic indicators. Source:[25].

1.6 The PVT computation

Once that the condition of lock of the tracking loops is achieved, the parameters are finely estimated and they can be employed to construct the pseudoranges. As mentioned in the previous section, the propagation time must be computed to construct the pseudorange, as the difference between the signal reception time, measured in the receiver time-scale, and the signal transmission time, measured in the GNSS time-scale. This misalignment introduces a bias on the pseudorange(2). Therefore, at least four pseudoranges are needed since four are the unknowns of the system (X_u, Y_u, Z_u) and the user clock bias δt_u.
It is important to underline that the structure of the data message is a part of the construction of the pseudorange. In fact, after that the carrier and the code are perfectly wiped off from the signal after the tracking, it is possible to correctly modulate the navigation message contained in the data bits. The navigation message contains information about the satellites position (ephemeris and almanac), satellites velocity and other information useful for the receiver. To give an example, the satellites velocity vector, contained in the navigation message, together with the pseudoranges allow to evaluate the user velocity.
Once the pseudoranges and pseudorange rates are computed, the PVT is estimated by means of mathematical methods, namely the Least-Squares (LS) and Weighted-Least-Squares (WLS) approaches or a Kalman filter. The PVT construction is not the main focus of this work, more detailed information is available in [13].
Regarding the quality of the PVT estimate, it depends on various aspects. As already discussed in section 1.1.1, the first factor to be considered is the number of satellites in LoS. The more the number of satellites, the lower the GDOP, the more precise the estimate. The GDOP is not only influenced by the number, but also on the geometry of the satellites. In fact, it can be demonstrated that if the satellites are distributed as a regular polytope, the GDOP is minimized corresponding to a more accurate PVT estimation. Note that the larger the number of satellites in view is, the more likely a regular polytope volume can be obtained. Therefore, the possibility of choosing a geometry close to the one of a regular polytopes increases and so it does choosing a GDOP value closer to the optimal one [8].

Chapter 2

Use of GNSS in Space

2.1 Current positioning and navigation technologies exploited in Space

Space navigation is a large field where the race for improving reliability, cost, real-time, and accuracy never ends. The main navigation system currently employed is named Inertial Navigation System (INS). The INS relies on accelerometers, gyroscopes, and magnetometers which allows the spacecraft to update its inertial state without requiring measurements from the external environment. Thanks to the inertial states over time, positioning can be performed by integration. However, this navigation system works only if the inertial state receivers are frequently and precisely updated by an external source, since, by nature, this technique strongly depends on initial state solution bias and noise inherent to inertial systems. Therefore, the navigation solution error drifts significantly over time.

In order to have an external update, the spacecraft relies on a communication link with a global network of ground tracking stations, initiated by NASA with the Deep Space Network (DSN) and followed by ESA with the European Space Tracking (Estrack) network. The network is composed by huge antennas that allows to estimate spacecraft's position and velocity thanks to radiometric measurements. An example of radiometric measurements are range, Doppler measurements and Very Large Baseline Interferometry (VLBI) [16]. These techniques function effectively and ensure an accuracy down to tens of meters. Nevertheless, they present several drawbacks. Firstly, the navigation process cannot be performed real-time, thus it is not usable for critical operations. Secondly, the spacecraft navigation completely relies on ground segment not autonomously, making the system very expansive.

Alternatively, the state estimation can be performed on board of the spacecraft allowing to have onboard autonomous navigation. Different technologies were implemented on this direction such as the Celestial Navigation via the use of Optical techniques and Pulsar X-rays [17][18].

In parallel, the GNSS systems could represent a validate alternative. Figure 2.1 shows the comparison between the presented techniques. We can note that GNSS method is dominant on many levels [16][17][18]. The mentioned fact justifies the nowadays growing interest to test and extend GNSS systems to the moon and beyond. It is relevant to underline that a step forward in the deep-space exploration is the investigation of sensor fusion so that all these technologies and their benefits are employed concurrently through the use of a Kalman filter.

Space Navigation Techniques Comparison	Autonomy	Order of accuracy [km]	"Real-time"	Cost	Size
Radiometric Tracking (DSN)	✗	1e-3	✗	✗	✓
X-Ray Pulsar Navigation	✓	1	✓	?	✗
Celestial Optical Triangulation	✓	10	✓	✓	✓
Full-Disk Optical Navigation	✓	10	✓	✓	✓
GNSS Navigation	✓	1e-2	✓	✓	✓
Inertial Navigation	✓	✗	✓	✓	✓

Figure 2.1: Comparison between Space Navigation Techniques.

2.2 State-of-the-art GNSS receivers for space applications

GNSS systems were originally planned to provide Positioning, Navigation and Timing (PNT) for terrestrial users. Nowadays, the trend is to extend the way we use GNSS signals, enabling space applications. The benefits to extend the GNSS use to high-Earth orbit and in lunar space are several:

- *Enable autonomous navigation in real-time*: Spacecraft can use the GNSS signals to obtain PVT information which is critical to mission operations, allowing many satellites the autonomy to react and respond to unforeseen events in real time and ensuring the safety of the mission;
- *Reduce tracking and operational cost*: GNSS receivers can also negate the need for an expensive onboard clock and simplifies ground operations, both of which can save missions money;
- *Provide timing source for hosted payloads*: GNSS allows to estimate even the time that can be transmitted to the independent attached modules of the spacecraft;

- *Enable a large number of scientific opportunities*: GNSS accuracy can help missions take precise measurements from space [14].

The use of GNSS at high altitude was analysed and discussed in *The Interoperable Global Navigation Satellite Systems Space Service Volume booklet.* To go into details, the Space Service Volume (SSV) is defined as the region of space extending from 3,000 km to 36,000 km altitude from Earth [15]. The SSV is partitioned in two in two different domains based on the peculiar characteristics in terms of geometry and signal availability. The two regions are the Lower SSV for medium Earth orbit and the Upper SSV for geostationary and high Earth orbits. The former, covering altitude from 3,000 km to 8,000 km, is characterized by orbit lower than GNSS satellites allowing an increased signal availability with the use of both zenith and nadir-facing antenna. Differently, in the latter the signal cannot be received from the spacecraft zenith, but just from nadir-facing antenna and most signals travelling across the limb of the Earth since the orbits are GEO orbits. The mentioned limitations on the signal reception translates in a significant reduction of the signal power level and availability. To overcome and improve these critic aspects an intereopable GNSS SSV is introduced, meaning that signals coming from different constellations can be exploited concurrently. Furthermore, the use of adequate antenna and advanced signal processing techniques could allow you to have a weak GNSS signal reception beyond the defined SSV (Figure 2.2). As discussed before, the interest to exceed the SSV up to the Moon and beyond is escalating but extending the use of GNSS at higher altitudes is an unexplored field and even if the recent studies are encouraging, still no guarantees are present. Despite the elevated prospects (Section 2.2), some questions remain opened on the feasibility to the GNSS system to correctly work at higher altitude. The starting point is to the test the existing Earth GNSS systems and then to implement a deep-space constellations in case of promising results. However, GNSS in space presents critical aspects that must be taken into account:

- *Weak GNSS signal power*: extremely low power levels because of Earth's umbra and long distances (Figure 2.2). Furthermore, the area eclipsed by earth leads to substantial power differences between main satellite antenna lobes and secondary ones which results in a threat to the acquisition of the weak signals due to the presence of strong GNSS signal with similar dynamics.

- *Poor satellites geometry*: due to high altitude, the satellites availability and satellites geometry are poor meaning that the values of GDOP are significantly higher. High GDOP values translates in less precise PVT solutions (Section 1.1.1).

- *High dynamics*: bigger relative velocity between the satellites and the receiver. High spacecraft speed is responsible for higher values of Doppler shift and rate with a consequent increase of the size of the SS during the acquisition. Furthermore, at this velocity the satellites in LoS changes quickly and the receiver has a shorter time to track each satellite. This might require a different selection logic and tracking loop design in order to cope with this more dynamic environment that will be discussed later during this chapter.

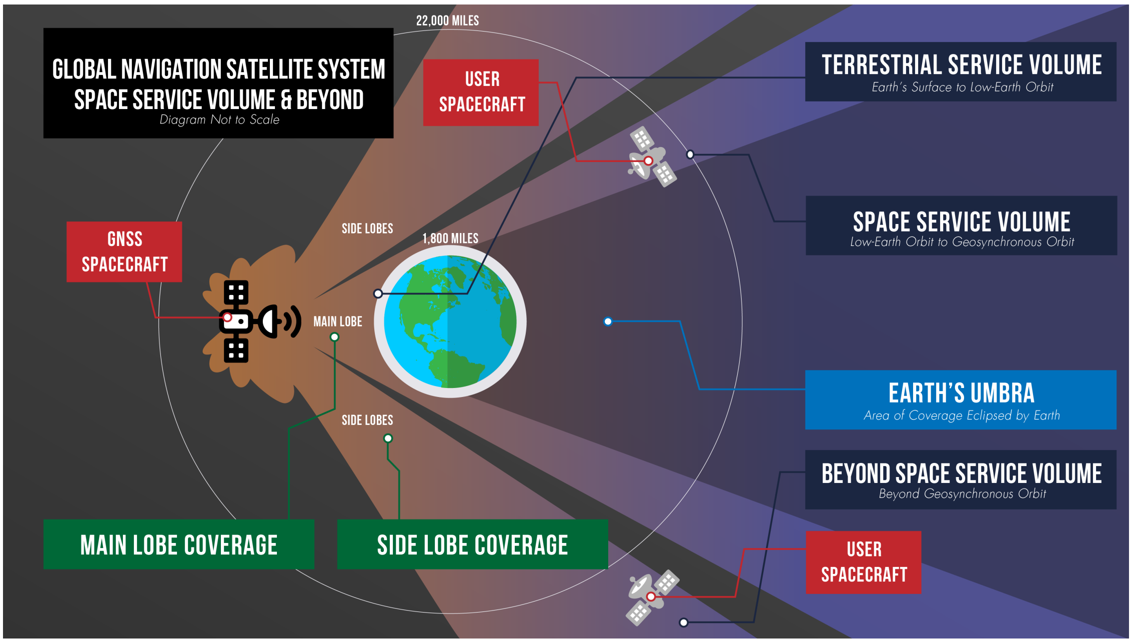

Figure 2.2: A graphic detailing the different areas of GNSS coverage. Source: [14]

2.3 Techniques for weak GNSS signal acquisition

As already discussed earlier, the space represents a challenging environment for the GNSS signals. In space scenarios, where the power level is extremely low and the geometry is poor, the GNSS receivers could not works properly. Advanced signal processing techniques are then employed making the receiver more robust against smaller value of C/N0. We refer these receivers as high sensitivity GNSS receivers.
Concerning the acquisition stage, as it has already been explained in chapter 1, it aims to find the best estimation possible of delay and Doppler shift, corresponding the maximum value of the CAF. Therefore, during this phase, research on the SS is done to find a peak emerging from the noise floor. The higher and the sharper the peak, the better the estimation of the parameters. However, if the power level is extraordinarily low as in case of space scenario, the noise floor could completely cover the peak leading to an acquisition fails (false detection). Therefore, advanced methods must be employed in order to reduce the noise level. Since the noise can be modeled as zero mean additive WGN, averaging operations can be performed for this purpose. Averaging can be done both before and after

the envelope. If the operation is applied before the envelope, it corresponds to a coherent time extension. Conversely, if the averaging is done after the envelope, it corresponds to a non-coherent accumulation.
Furthermore, external aidings can be employed to smooth the path of the acquisition stage, providing assistance information such as estimated Doppler shift and rate. In space applications, the assistance data are generally provided by an Orbital Filter (OF).

2.3.1 Coherent time extension technique

As already mentioned before, with the coherent time extension, the averaging operation is applied before taking the envelope of the CAF (20). This technique consists on increasing the value of T_{coh} by a factor of M

$$T_{coh} = M \cdot NT_s \tag{19}$$

where M is the number of coherent sums and T_s is the sampling time. The extension of the integration time corresponds to increasing the number of samples considered from N to MN.
Consequently, the CAF expression changes to

$$S(\bar{\tau}, \bar{f}_d) = \left| \frac{1}{M} \sum_{i=1}^{M} R^{(i)}(\bar{\tau}, \bar{f}_d) \right|^2 \tag{20}$$

Thanks to this strategy, the signal power level increases in a directly proportional manner to the coherent sums M. On the contrary, since the noise is a zero mean WGN, its power remains constant. The overall SNR is then increased by a factor of M.
To give an example, with an $M = 4$ meaning that the number of samples is quadrupled, the SNR growth about 6 dB. A higher SNR means that the gap between the noise floor and the peak increases as well. A sharper peak increases the chances to exceed the acquisition threshold resulting in a correct acquisition of the signal.
However, if the coherent integration time is increased, Doppler bin size grows (10). Hence, the SS is enlarged signifying that the time needed to perform the correlation operations increases. The conclusion is that besides the better acquisition performances, this method rises the complexity of the system and makes the process more time consuming. A further issue of the time extension is represented by bit transition. In fact, the navigation message contains data-bit transitions that can generate opposite signs of consecutive correlation blocks. If we are in an unlucky situation in which two peaks are summed opposite in sign, they canceled themselves. In this worst case scenario, the presence of a bit transition acts as a sort of subcarrier which splits the main lobe of the spectrum in two side peaks, symmetric with respect to the correct bin, leading to a wrong acquired Doppler frequency.
To minimize the probability to have bit transition the coherent integration time is then

limited by the bit length in the following way:

$$T_{coh} \leq \frac{T_b}{2} \tag{21}$$

so that the the transition cannot happen in two consecutive integration intervals.

2.3.2 Non-coherent time extension technique

In the non-coherent time extension, the averaging is performed after taking the envelope of the CAF (22). The correspondent expression of the CAF is:

$$S(\bar{\tau}, \bar{f}_d) = \frac{1}{K} \sum_{i=1}^{K} \left| R^{(i)}(\bar{\tau}, \bar{f}_d) \right|^2 \tag{22}$$

where K is the number of non-coherent accumulations. Therefore, with this technique we sum K instances of the basic ambiguity function. The CAFs are summed non-coherently, since the squared-envelope removes the phase dependence. As in the case of coherent extension, performing this operation grants an increase of the signal power level by a factor of K. However, the difference is that in this case even the noise power level increases. Since the noise samples are uncorrelated the noise power does not increase proportionally with K, but with $\sqrt{K}$ [19]. Hence, the overall SNR gain is damped by the mentioned fact meaning that it is lower than obtained with the coherent extension. This phenomenon is referred to as squaring loss and makes the non-coherent combination less effective than the coherent one.
However, the non-coherent accumulations do not suffer of bit transition that is the main limitation of the coherent technique. An optimal compromise is then using both coherent and non-coherent extension. The obtained CAF is:

$$S(\bar{\tau}, \bar{f}_d) = \frac{1}{K} \sum_{i=1}^{K} \left| \frac{1}{M} \sum_{i=1}^{M} R^{(i)}(\bar{\tau}, \bar{f}_d) \right|^2 \tag{23}$$

Combining these two techniques, the overall integration time is extended by a factor $K \cdot M$ where K is the number of non-coherent accumulations and M is the number of coherent accumulations. The design of these parameters cannot be done a priory, but the best trade-off depends on the specific situation of the receiver.

2.4 Techniques for weak GNSS signal tracking

The task of the tracking stage is to improve the accuracy and track over time the approximate estimations of the acquisition, so that the pseudoranges are accurately constructed and the navigation message is demodulated. However, several issues can arise if the environment is degraded as in case of high altitude. To give an example, one possible scenario is that the tracking loop could be not able to follow the signal since the Doppler drifts significantly over time due to the higher Doppler rate typical of a space scenario. Furthermore, even the higher noise level can lead to an unsuccessful signal tracking. For these reasons, the tracking needs to be made more robust against the noise and more sensitive to face high relative dynamics. On this purpose, the tracking parameters can be designed and modified in an optimal way to operate on this scenario and eventually different tracking architectures can be considered if needed. This thesis focuses on meticulously analyze and investigate the tracking performance on space environment to understand what processing is possible with the typical architecture optimizing the values of the tracking parameters. It is important to underline that as in case of the acquisition, even for the tracking stage the use of assistance information represents a fundamental advantage to be employed in a harsh space scenario.

2.4.1 Optimal parameter design

One important step to improve the tracking performances is to modify appropriately the parameters. This because the tracking parameters have a considerable impact on the characteristics of the tracking system. However, the proper design of the parameters is a challenging task since continuously trade-offs occurs. The reason behind this fact is that a paradox involves the three major components of the tracking architecture that are the integration time, the discriminator and the loop filter functions of the carrier tracking loop. A GNSS receiver to tolerate dynamic stress should have a short integration time, an FLL discriminator and a wide filter bandwidth. Conversely, to be robust against the noise and to be more accurate a GNSS receiver should have a large integration time, a PLL discriminator and a narrow bandwidth.
The integration time is the time over which the tracking parameters are evaluated, it is strictly related to the carrier loop bandwidth, analogue but opposite considerations can be done. The integration time is a compromise design. It should be extended as possible to operate under weak signal conditions. Differently, a successful tracking requires a short integration time as feasible to operate under high dynamic stress signal conditions. To summarize, a paradox must be solved during a GPS receiver design, between the integration time and and the loop filter bandwidth. In high dynamic conditions, a short integration is needed but PLL bandwidth should be wide. However, to tolerate low C/N0, the integration time should be long and the carrier loop filter noise bandwidth should be narrow, so that the measurements obtained are more accurate. In practice, some compromise must be made to resolve this paradox [25].

For example, about the discriminator, as already discussed in section 1.5.1, a PLL assisted by an FLL generally works well than having just one of the two. A deeper analysis of these parameters will be done in the next chapter where different values of them will be tested on a simulated space scenario trying to design optimally them.
However, as we have seen, in a harsh environment as space both issues on dynamics and noise are present. Therefore, changing the parameters could be not enough to successfully track the signal. Alternative tracking architectures and external aiding are then considered on this purpose.

2.4.2 Open loop architecture

An alternative architecture to the closed loop already presented (Figure 1.9) is having an open loop batch processing approach (Figure 2.3). The main feature of this kind of approach are studied and discussed in [26] and can be summarized as follows:

- *Improved signal observability as compared to sequential processing*: the signal is not processed sample-by-sample, but by means of batch of data. Thanks to this parallel estimation techniques can be applied such as parallel time domain, frequency-domain, and joint time frequency-domain estimation computations granting an improvement of the signal observability. Therefore, the receiver is able to better visualize and estimate strong changes in frequency in case of high-dynamic environment;
- *Capability of parallel computations*: the batch processing approach enables parallel computations on the batches of samples. Parallel correlation computations can be applied by means of frequency-domain correlation techniques. Two examples of this are present in [27][28]. The first consists in a computation of the Doppler shifts from the search space in parallel thanks to the FFT. The second is the parallel correlation computation for the entire GPS CA code search space using FFT and IFFT;
- *Improved tracking robustness as compared to closed-loop sequential tracking*: the open-loop tracking architecture is more robust as compared to the sequential closed-loop one. To be more specific, batch processing computes the entire image of the signal, which allows immediate tracking recovery after a temporary signal loss. Moreover, the receiver using batch processing approach does not have to follow the motion dynamic within the bandwidth of the filter, but within a correlator bandwidth. The latter is significantly wider than a loop-filter bandwidth, hence the open-loop superior tolerates high dynamic stress.

Given the above powerful advantages of batch processing, why would one still need to use the sequential closed-loop algorithms. The answer is given by the computational efficiency of sequential processing techniques. Sequential processing allows for minimization of memory and computational resources. Contrary to batch processing, it does not require additional computational resources to increase resolution of signal parameters.

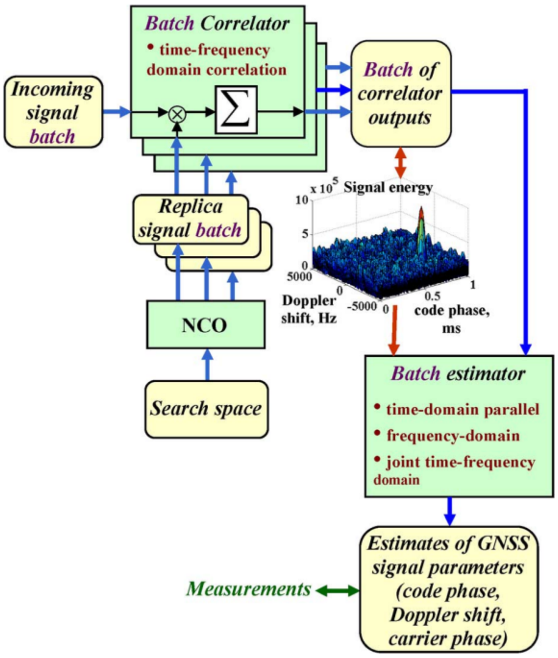

Figure 2.3: Block diagram - Open loop tracking architecture. Source: [26]

2.5 The Orbital filter: an external aiding

External aidings are fundamental to face the harsh space environment characterized by poor geometry and reduced visibility. Furthermore, the relative dynamics between the receiver and the transmitters are definitely higher than the routine values for terrestrial applications. As a consequence, the GNSS space signals suffers from larger values of Doppler shifts and Doppler rates making the traditional GNSS receivers unable to correctly perform the acquisition and the tracking stage.
Therefore, assistance information regarding these values must be provided to the GNSS receiver through a more advanced architecture. An example of this is the use of an adaptive Orbital Filter (OF) to aid the acquisition and the tracking of very weak signals leading to a higher accuracy on the navigation solutions. An orbital filter based on an adaptive extended Kalman filter is presented in [20]. To be more specific, the orbital filter is a GPS-based filter for lunar mission able to propagates the kinematic state of the spacecraft during the orbit, through the MTO. Based on the altitude of the receiver, different propagation models are present considering gravity perturbations. The OF filters provides as output the Doppler shift and the Doppler rates that are, in turn, employed by the GNSS receiver to improve the execution of acquisition and tracking stages. The iteration process of the orbital filter on board of the receiver determines the rate at which

the outputs can be provided to the GNSS signal processing architecture. The mentioned paper shows that the use of this kind of filter is significantly beneficial for the GNSS space processing since the sensitivity and robustness of the receiver is improved. Thanks to this, the GNSS receiver can operate even at higher altitudes, potentially up to the Moon and beyond.
The impact of employing an orbital filter on the acquisition and tracking was even shown in other studies [21][22][23][24]. All of them goes on the same direction arguing that the OF is gainful and profitable for the GNSS receiver for space applications.
The reason for this is that the values of the Doppler provided by the filter are used as a starting point from the GNSS receiver. Having an estimate of the Doppler means reduce the search space of the Acquisition, making the process faster and more precise. Consequently, even the tracking stage can benefit from a more accurate value of starting Doppler meaning that there are more chances to track the signals and to do that in a lower amount of time.

Chapter 3

Use of GNSS to the Moon

The lunar exploration is becoming again strongly attractive. Current lunar exploration efforts involve more than eighty national space agencies and several private companies and partnership, making the Moon again a top space exploration priority.
International Space Agencies Meet to Advance Coordination in Space Exploration of Moon and Mars On 30th November and 2nd December 2021, senior managers representing 24 space agencies met virtually for a meeting of the International Space Exploration Coordination Group (ISECG). The purpose was the promotion of coordinated efforts in space exploration of the Moon and Mars as per the Global Exploration Strategy [29]. As already mentioned in chapter 2, the GNSS role can be fundamental for lunar exploration in enabling autonomous navigation, reducing mission costs and so on. The GNSS applications on the lunar exploration are numerous:

- Lunar Surface Operations, Robotic Prospecting and Human Exploration;
- Human-tended Lunar Vicinity Vehicles (Gateway);
- Robotic Lunar Orbiters, Resource and Science Sentinels;
- Earth, Astrophysics and Solar Science Observations;
- Satellite Servicing;
- Lunar Exploration Infrastructure.

On this direction, the U.S. National Aeronautics and Space Administration (NASA) planned three lunar exploration plans: Artemis, Gateway and Commercial Lunar Payload Services.
Artemis is the name of a NASA mission which the primary goal is to bring back the human presence on the lunar surface. The reasons to return back on the Moon are several such as scientific discovery, economic benefits, and inspiration for a new generation of explorers [30]. An important part in frame of the Artemis program is the need to have positioning

and time of the lunar orbiting station (Gateway) and to facilitate future colonization of the Moon and beyond. One important step on this direction is represented by the Navigation Early Investigation on Lunar surface (NEIL). Presently the highest altitude at which it was computed the position of a spacecraft using GNSS satellites is 200,000 km, almost half-way to the Moon. This success, reached by NASA in 2019 with the Magnetospheric Multiscale (MMS) spacecraft, suggests the possibility of the employment of GNSS for the spacecraft navigation as far away as the moon. Consequently, NEIL is presumed to be the first receiver testing the positioning with both GPS and Galileo systems almost 400,000 km away from Earth. As a result, as mentioned before, NEIL represents a crucial advance to apply GNSS timing and positioning for the future Moon missions such as, the deployment of lunar rovers, satellite constellations, lunar space station Gateway and all the infrastructures needed for the Artemis missions. To be more specific, the receiver will be the result of a collaboration between the U.S. National Aeronautics and Space Administration (NASA), the Italian Space Agency (ASI) and the Italian firm Qascom srl. Qascom's aim is to develop a GNSS reception system for ASI, consisting of a dual-frequency and dual-constellation receiver and the entire signal reception chain (antenna, LNA, filters), capable of supporting the extreme conditions of the moon. The NEIL payload will be integrated into the Lunar GNSS Receiver Experiment (LuGRE), a cooperation framework defined in the agreement between ASI and NASA, aiming to develop activities in lunar and cislunar environments.

3.1 The LuGRE project

LuGRE will fly during a crucial and highly active period for lunar navigation advancement. NASA and others view GNSS as a crucial enabling technology for cislunar and lunar navigation, particularly in the near future. NASA and the European Space Agency (ESA) have published plans for lunar communications and navigation infrastructure that will provide one-way radionavigation signals in lunar orbit, addressing the visibility, geometry, and signal-strength limitations of using solely Earth-based GNSS. A phased approach is required to develop both capabilities and transition between them. First, flight demonstrations must demonstrate the dependability of using GNSS for lunar navigation. Next, operational lunar GNSS receivers will be flown to establish the capability at Technology Readiness Level (TRL) 9 ("flight proven") , after which they will be commercialized or further developed to meet the wide range of mission requirements, from flagship-level receivers to integrated chipsets incorporating both GNSS and lunar-vicinity navigation signals. Then, this technology can be incorporated into lunar activities as standard equipment, enabling fully integrated real-time navigation from near-Earth to the lunar surface. It is anticipated that LuGRE will satisfy the first step of this strategy, allowing for the full utilization of GNSS for lunar navigation.

LuGRE is a mission that is part of NASA's Commercial Lunar Payload Services (CLPS), and it consists of 9 scientific and technological experiments that will be conducted on the moon. The launch of the mission is planned to take place using a Space X Falcon 9 rocket at the tail end of 2023. The LuGRE receiver as well as the antenna will be incorporated into the Firefly Blue Ghost 1 lander. The primary objective of LuGRE is to extend GNSS-based navigation to the Moon, and it will accomplish this by completing the following steps: The first thing that needs to be done is to set up a receiver on the moon so that GNSS signals can be picked up there. The next step is to analyze the carrier-to-noise ratio of the signals that were received, spectral density, signal availability expressed as the typical number of satellites in line of sight, the presence of GDOP, and multipath caused by the lunar surface. Second, the quality of the obtained navigation solution should be characterized by measuring the amount of time it takes to reach the first fix as well as the navigation solution over time. In addition to that, GNSS Data Collection while in transit is another significant part of the mission. In point of fact, in addition to functioning as a typical real-time receiver, NEIL will also be collecting and delivering transit raw IQ data to the GNSS community as well as the science community. After the data have been collected, they will be used to help develop GNSS receivers that are tailored specifically for use on the moon [31].

To be more specific, a high-gain L-band antenna, a low-noise amplifier, and a weak-signal Global Navigation Satellite System (GNSS) receiver are all integrated onto the Firefly Blue Ghost lander to make up the flight payload. The payload is going to be responsible for receiving and tracking GPS L1 C/A and L5 signals, as well as Galileo E1 and E5a signals. It will also produce pseudorange, carrier phase, and Doppler measurements. Real-time navigation, least-squares point solutions, and onboard filter solutions will all be produced by the receiver. Other telemetry will include the number of signals that can be seen and followed, the degree to which precision has been diluted, and the carrier-to-noise density ratio (C/N0). Additionally, the receiver has the ability to record brief stretches of raw L1 and L5 I/Q baseband samples. These samples can then be downlinked and later replayed as input to a ground-based receiver. The receiver also has the capacity to record short spans of I/Q baseband samples. On the lunar surface as well as while the spacecraft is in transit between Earth and the Moon, LuGRE will perform its operations [32].

Preliminary examination of the LuGRE operations shows that there is a high degree of signal visibility throughout the mission, with an average of four GNSS signals visible even on the lunar surface [32]. The transit phase analysis demonstrates the ability of an extended Kalman filter to handle pseudorange measurements and converge within the available time during transit operations periods. Furthermore, the possibility to acquire signals in postprocessing utilizing downlinked raw I/Q baseband samples is confirmed. The LuGRE Science Team has identified ten science investigations that will drive data processing and product development, as well as more than a dozen more that will be done as best effort.

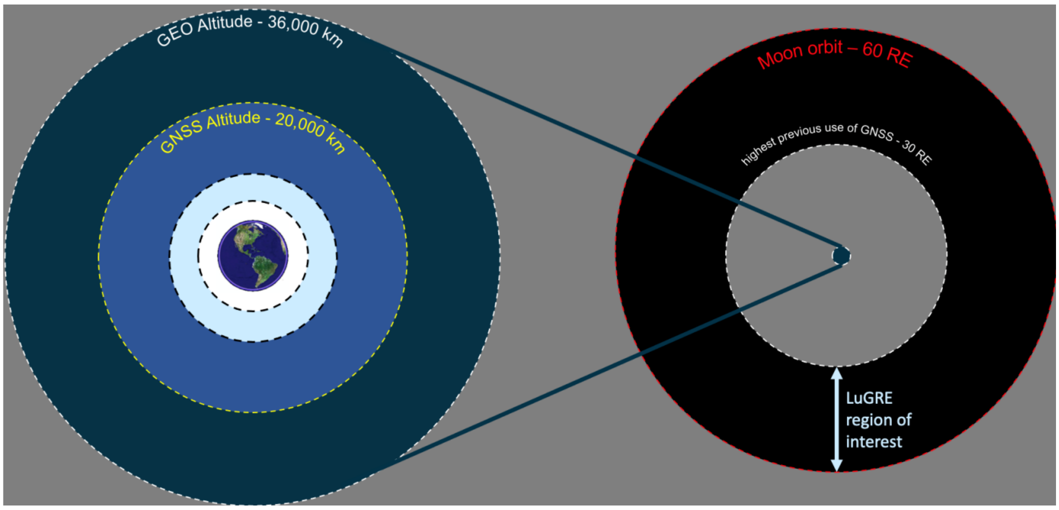

Figure 3.1: LuGRE region of interest. Source: [31]

Figure 3.2: Official LuGRE logo. Source: [31]

3.2 Processing of IQS

Part of the time window available during the orbits will be dedicated to data collection in transit. These data collected will be downloaded as IQ samples and then used to perform post-processing by the science community. IQ sampling consists in transmitting two sinusoidal waves, one called in-phase component (I) corresponding to the cosine wave and the other called in-quadrature (Q) component corresponding to a sine wave or in general 90 degrees out of phase with respect I. From the transmitter point of view, instead of transmitting one single sinusoidal wave, we transmit the I and Q components summed together. In this way, the signal transmitted has the following form

$$x(t) = Icos(2\pi ft) + Qsin(2\pi ft) \tag{24}$$

However, a trigonometry identity say to us that when we add a sine and cosine function, we get another pure sine wave with a different phase and amplitude. This ability is extremely useful as a transmitter because we know that a sinusoidal signal must be transmitted for an electromagnetic wave to travel through the air. Furthermore, when compared to adjusting both an amplitude and a phase, adjusting two amplitudes and performing an addition operation is a significantly simpler process than adjusting one amplitude and one phase. From the receiver side, using two ADCs, we sample the I and Q branches separately before combining the pairs and storing them as complex numbers. In other words, you will sample one I value and one Q value at each time step and combine them using the formula $I+jQ$. In other words, each IQ sample yields one complex number.

The reasoning for complex sampling is that IQ samples enable multiple functions, which can be summed up as follows:

- *Record and replicate the remote scenario*: possibility to perform in-lab replication of the RF conditions at the in-space receiver front-end;
- *Perform additional advanced signal processing*: possibility to run advanced signal processing algorithms for further analysis such as feature extraction and detection of outliers. Furthermore, pre-processing can be applied to the recorded signals trying to obtain a data "cleaning" by means of denoising techniques;
- *Perform Acquisition/Tracking engine research*: IQ samples can be employed as test-bed data for future digital signal processing algorithms aimed to improve the acquisition and tracking performances;
- *Risk mitigation*: IQ samples processing can be employed to asses the quality of the GNSS signal in both time and frequency domain.
  - In time domain: time series of GNSS signals can highlight anomalies such as unwanted modulation effects in the dynamics of the received signal. Histograms

of the recorded IQ samples return an estimation of the probability density function of the quantized samples and shows possible distortions due to unexpected dynamics of the signals.

  - In frequency domain: representation of transformed signal allow to assess the spectral behaviour and possible presence of outliers due to propagation environment or radio-frequency interference

  Moreover, the results obtained by IQS processing could be cross-validate with the results of the on-board processing.

- *Employ the flexibility of the software receiver*: the software receiver is not hardware-constrained so that it gives the possibility to test different configurations of the parameters and algorithms for acquisition and tracking loops. In addition, the receiver can exploit signals and constellations not currently supported by the in-space receiver.

In addition to the benefits that have been suggested, the processing of the IQ samples is characterized by a variety of constraints. In the beginning, the IQ samples are conditioned by the front-end characteristics such as the bandwidth, A/D features, noise, and antenna. Second, and possibly more importantly, concerns regarding the limitations of data storage and transmission. For this reason, the next chapter will be dedicated to investigate the best possible compromise on the parameters of the data that were collected, such as the IQS duration, the sampling frequency, and the number of quantization bits.

3.3 Introduction to snapshot positioning

The data collected during the trajectory are just very brief interval (few milliseconds) of the received satellite signal due to cost limitation of the mission. Find the order of magnitude of this interval is one of the main task of this thesis. On this purpose, several experiments was performed and they will be presented in chapter 4.

In general, Snapshot positioning is defined as the technique to determine the position of a GNSS receiver using only a very brief interval of the received satellite signal. To make this possible, the mentioned technique does not demodulate the navigation message; rather, it attempts to estimate the critical parameters, such as the time of week, that are necessary for the construction of the pseudoranges. This technique shows more advantages in applications that require timely positioning results or when energy consumption is significantly limited. For example, in mass market IoT applications is significantly increasing the need of snapshot positioning algorithms due to the stringent constraints of battery-powered IoT devices. The advantages on operate only on an interval of the received signal are different.

1. *Energy efficiency*: the main improvement led by snapshot positioning is the decrease in power consumption [33];
2. *Economic cost*: it was largely demonstrated that snapshot positioning ensures a gain in terms of money compared to conventional techniques [34];
3. *Positioning accuracy*: the innovations and new algorithms are continuously arising motivated by the enormous potential applications of this technique.

During the post-processing of the IQS, the scientific community may take into consideration and make use of this method in an effort to take advantage of the many benefits available.

Chapter 4

Processing of GNSS signal at the Moon

The purpose of this chapter is to conduct a preliminary analysis of a GNSS receiver while it is traveling on the trajectory to the Moon and to gain an understanding of the types of processing that are possible given a specific amount of time for the IQS. Following this, the information regarding the duration of the snapshot can be used as a reference in order to effectively design the data that was collected during the orbit of the NEIL receiver. The first part of this chapter is dedicated to analyze and process the IQS provided by the Qascom simulation. The aim of the analysis is to understand what processing is possible having the IQS of a given duration. This allows to design an acceptable and reasonable value of the size of the snapshots taking into account the agreement limitations. The IQS provided by Qascom emulates the signals sent by the receiver at three different points of the trajectory corresponding to the distances: 30RE, 45RE and 60RE. The specific of the Qascom signals are reported in Table 4.1.
The sampling frequency is 8 Msps and the number of quantization bits are 8 in all the three cases, while the duration of the signal is 400 ms at 30RE and 1 s at 45RE and 60RE. The GPS L5 and GALILEO E5 are not considered in this analysis.

	30RE	**45RE**	**60RE**
fs [Msps]	8	8	8
qBits [bits]	8	8	8
duration [ms]	400	1000	1000

Table 4.1: The specific of IQ Qascom samples GPS L1/GAL E1.

Following this, the Qascom scenario is simulated using N-FUEL, which enables a more in-depth analysis on the tracking performances thanks to the capability to replicate and generate the signal under a variety of different conditions. N-FUEL is a signals and disturbances simulator that has been implemented as a set of non-real time MATLAB functions. It is able to simulate the raw GNSS signal samples that a GNSS receiver would see after analog-to-digital conversion has been performed on them. In addition to that, it comes with tools for plotting and analyzing data. N-FUELS has been developed by the Navigation Signal Analysis and Simulation (NavSAS) group, a joint research team of Istituto Superiore Mario Boella and Politecnico di Torino.

However, it is essential to emphasize that a GNSS receiver has never been validated at such great distances, which means that there is no GNSS signal to be processed at this time. As a result of this, it is necessary to create a simulation of the space environment that is as accurate to the real one as is possible.

All the signals were processed by means of the NavSAS software GNSS receiver which architecture is shown in Figure 4.1.

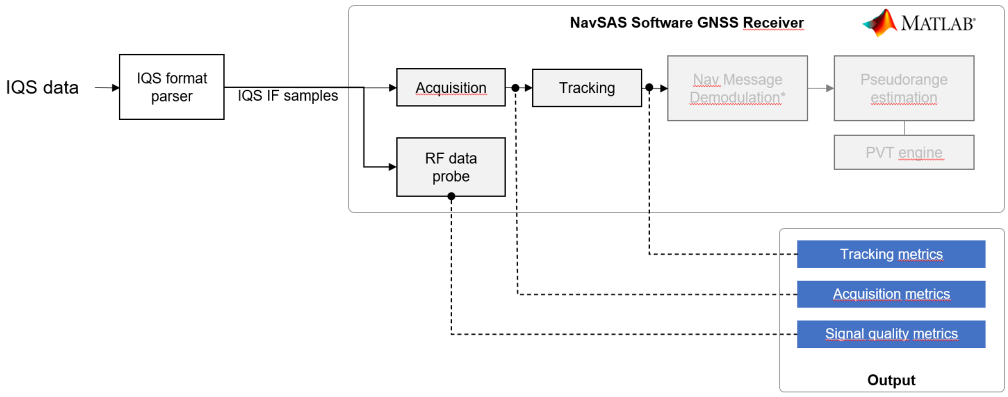

Figure 4.1: IQS processing architecture

4.1 Simulation environment

The first step is then focused on the simulation environment. In doing so, a link budget calculation is computed given that NEIL trajectories are available in advance. From the trajectories information about the receiver distances can be retrieved. The link budget computation takes into account all of the power gains and losses that the GNSS signal experiences during the mission. A link budget equation generally is of the form:

$$P_{\mathrm{RX}} = P_{\mathrm{TX}} + G_{\mathrm{TX}} - L_{\mathrm{TX}} - L_{\mathrm{FS}} - L_M + G_{\mathrm{RX}} - L_{\mathrm{RX}} \tag{25}$$

where P_{RX} is the received power, P_{TX} the transmitter output power, G_{TX} the transmitter antenna gain, L_{TX} the transmitter losses such as connectors or cables, L_{FS} the path loss L_M other kind of losses such as fading,polarization mismatch. G_{RX} is the receiver antenna gain and L_{RX} the receiver losses, again connectors or cables. All the quantities are measured in dB. The path loss is the loss due to propagation between the transmitting and receiving antennas and it is usually modeled by a simplification named free-space path loss. The free-space path loss is the attenuation that would result from a line-of-sight path through free space, in absence of obstacles and then with no reflection or diffraction. The free-space attenuation formula can be derived starting from the Friis transmission formula and it is:

$$L_{FS} = \left(\frac{4\pi df}{c}\right)^2 \tag{26}$$

$$L_{FS}[dB] = 20\log_{10}\left(\frac{4\pi df}{c}\right) = 20\log_{10} d + 20\log_{10} f + 20\log_{10}\frac{4\pi}{c} \tag{27}$$

where d is the distance between the two antennas, f is the signal frequency and c is the speed of light. We can note that the attenuation is directly proportional to the distance, so that the greater the distances, the lower the power received, typical case of a space scenario. Returning to our case, the information about the distances can be retrieved from the trajectories and even the information about the antenna as the gain are available. Therefore, a model can be defined to describe the behavior of the C/N0 versus the receiver distance during the different phase of the mission. Based on all of these information Qascom generates IQ samples to be similar as possible to that that will be sent by the receiver during the orbit to the lunar surface.

4.2 IQS processing: Acquisition stage

The acquisition stage comes first in the process of analyzing the IQ samples. In other words , the objective is to first successfully acquire at least one satellite, then successfully acquire the maximum number of satellites possible, and finally figure out the order of magnitude of the signal duration required to successfully carry out the steps in the previous sentence. Due to the fact that the acquisition stage comes before the tracking stage, there is no way to perform tracking if the rough estimations of the acquisition stage are not available, as was covered in Chapter 1.

A preliminary analysis reveals that we are unable to acquire any satellites by following the traditional acquisition procedure. This finding supports the hypothesis.As a result, strategies for the acquisition of weak GNSS signals are being considered (already presented in section **??**). To provide further clarity, the time extension utilizes not only a coherent but also a non-coherent approach.

The coherent time extension could allow a peak exceeding the acquisition threshold since through the coherent sums the signal power is increased proportionally to the time extension. Differently, the noise is not affected by this operation if it can be modeled as a White Gaussian Noise (WGN) with zero mean. Therefore, the overall SNR is increased

as the signal power, granting a better distinction between the correlation peak and the noise floor (a more detailed explanation is present in Chapter 2). In the end, a value of coherent time extension of 10 milliseconds is chosen for GPS and 12 milliseconds is chosen for Galileo respectively, and a number of non coherent accumulator equal to 6 is chosen, all of which are based on the results of the experiments.
The Figure 4.2 shows the acquired GPS satellites on L1 at 45RE both with an without time extension.
As anticipated before, we are not able to acquire any satellite when the coherent integration time is equal to the code period as depicted by Figure 4.2a. Differently, Figure 4.2b shows that thanks to the extension of the integration time up to 10 ms, two satellites are successfully acquired .
The same discussion can be repeated for each distance and for each signal at the same distance available. Tables 4.2 and 4.3 reports the total number of satellites acquired respectively for GPS L1 and Galileo E1c signals. It is important to underline the for 30RE and 61RE only one signal was processed, while for 45RE and 60RE we have respectively two and four signals available. We can observe that the coherent time extension is beneficial in each situation even in it is less evident for Galileo signal at short distances. This can be explained by the fact that Galileo has longer codes than GPS (4ms versus 1ms) which translates in an advantage in terms of acquisition performances.
Moreover, as expected, the average number of satellites acquired decreases by increasing the distance given that longer distance means a weaker signal received.
In terms of the duration of the signal, the findings indicate that a duration of the signal between 50 and 100 milliseconds is sufficient to acquire the most powerful satellite for each distance to Earth; this is the case even on the surface of the Moon. We are able to draw the conclusion that IQ sample durations on the order of one hundred milliseconds should make it possible to successfully acquire at least one satellite.

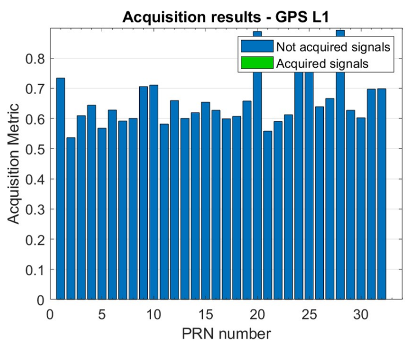

(a) Tcoh = 1 ms, zero satellites acquired

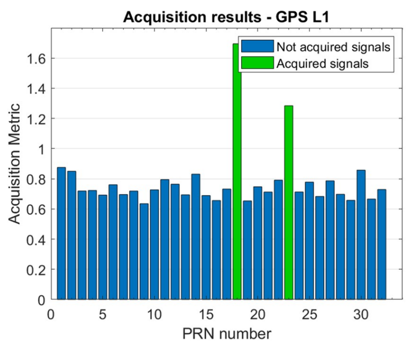

(b) Tcoh = 10 ms, two satellites acquired

Figure 4.2: Acquired GPS L1 satellites of IQ Qascom samples at 45 RE.

	30RE	**45RE**	**60RE**	**61RE MSO**
Tcoh = 1ms	1	0	0	0
Tcoh = 10ms	4	3	4	2

Table 4.2: Number of GPS (L1) satellites acquired versus the distance processing Qascom IQS.

	30RE	**45RE**	**60RE**	**61RE MSO**
Tcoh = 4ms	1	3	0	0
Tcoh = 12ms	4	3	4	0

Table 4.3: Number of GAL (E1c) satellites acquired versus the distance processing Qascom IQS.

4.3 IQS processing: Tracking stage

After characterising the acquisition, the next step is to perform and analyze the tracking stage. As mentioned before, the tracking is the main focus of this thesis, consequently a deepened analysis is presented. As already discussed in Section 1.5, the tracking is the most complex part in a GNSS receiver due to the presence of a crossed double loop. Therefore, characterizing the outcome of the tracking is a challenging task and it is not available a standard and unique way to comment and quantify a quality of a tracking results. During this experiment a Phase Lock Indicator (PLI) is considered. The Phase Lock Indicator was presented in section 1.5.3. A Phase Lock Indicator of 0.766 is taken as the acceptable threshold, which corresponds to a phase error of 20°. This proposed value of the PLI threshold is based on tracking results obtained during a preliminary analysis. Therefore, the samples with a Tracking lock indicator less than the threshold are indicated as loss of tracking points allowing the comparison of different tracking outcomes.
A Time to Lock (TTL) is proposed based on the PLI computation to understand the order of magnitude of the time needed for the tracking estimation. The TTL is defined as the first time at which the the condition of lock is achieved, meaning that the tracking structure is able to follow the quantity the Doppler and the delay of the incoming signal. The decision logic was designed performing preliminary experiments. This is the following: the TTL is computed in correspondence of the first of five consecutive PLI values over the threshold during the tracking loop. In other words, the lock is declared when the PLI is greater than the PLI threshold for five successive tracking loops and the time of convergence is evaluated at the first of these samples. A sequence of values above the threshold is used to increase the lock declaration robustness taking into account the PLI values fluctuations also under the considerations taken in section 1.5.3. The FLL time is added to that evaluated with the PLI when the FLL-assistance is present. In other words, the software receiver gives the possibility to have the FLL loop before going on the PLL

processing. As already discussed in Section 1.5, FLL provides a more accurate value of frequency allowing the PLL to work on a narrow band which results in a shorter transient time and then to achieve the convergence in a lower amount of time. However, during the FLL stage the tracking cannot converges and then the FLL time must be considered as an additional time needed for the tracking stage.
The proposed lock declaration is further validated trough a visual check on the tracking plots.

4.3.1 Tracking performance depending on PLL bandwidth

The PLL is one of the major component of the tracking phase, as already discussed in section 1.5. As a matter of fact, the PLL bandwidth plays a crucial role in the tracking performances.
To be more specific, if the carrier loop filter bandwidth bandwidth is enlarged, the receiver is able to track the values at stake with greater chances, since it increases the ability to tolerate dynamic stress. In other words, the condition of lock is achieved with an higher probability. However, in the other hand, a large bandwidth means a large window in which more noise will enter in, which translates in a carrier estimate less accurate. Consequently, the reason to maintain a lower value of bandwidth is to reduce the noise component of the signal.
In choosing the PLL bandwidth the trade-off between the reduction of the noise and the ability to tolerate dynamic stress should be taken into account. In case of low C/N0 as in a space scenario, since the noise has an higher power than usual, the typical values of PLL bandwidth used could be not enough to track the weak signal. A simulation for different C/N0 in a space environment is performed in order to choose a proper value of PLL bandwidth for each situation. The results shows that a value of 15 Hz works appropriately for C/N0 in the order of 40 dB-Hz and above. However, the bandwidth must be reduced to 10 Hz in order to track the signal for values of C/N0 from 25 to 40 dB-Hz. Figure 4.3 depicts two different tracking outcomes with respectively 10 Hz and 15 Hz of carrier loop filter bandwidth for a C/N0 of 38 dB-Hz. The figure shows the changes in the values of correlator outputs $Q_{k,d/p}, I_{k,d/p}$, raw and filtered PLL discriminator output $\delta\varphi_k$, prompt, early and late correlator results and raw and filtered DLL discriminator output. We can notice that I and Q correlator outputs of the picture on left cannot be distinguished and the points of the discrete-time scatter plot of IQ are distributed as a cloud. This is the typical output of a tracking fails, where the lock condition is not achieved. Therefore a bandwidth of 15 Hz does not make the tracking to converge for a C/N0 of 38 dBHz.
The ideal scatter plot is that with all the points with plus and minus 1 for I, representing the bits of the navigation message and zero for Q. In this specific case, since the signal under test is E1c that is the pilot signal, the scatter points converge randomly or on 1 or -1 of the I prompt correlator. In the outcome with a bandwidth reduced to 10 Hz, the scatter points shows a trend similar to the ideal one, indeed the points are distributed

around plus 1 of the I prompt correlator.
If the conditions are weaker, a further restriction of the PLL bandwidth is needed. Figure 4.4 depicts two different tracking outcomes with respectively 1 Hz and 10 Hz of carrier loop filter bandwidth for a C/N0 of 24 dB-Hz. The figure shows again the changes in the values of correlator outputs $Q_{k,d/p}$, $I_{k,d/p}$, raw and filtered PLL discriminator output $\delta\varphi_k$, prompt, early and late correlator results and raw and filtered DLL discriminator output. By repeating the same considerations on the previous figure, we can conclude that in this case a PLL bandwidth of 10 Hz is not sufficient to achieve the tracking lock. Conversely, reducing the bandwidth to 1 Hz, the tracking preforms successfully since two clouds are presented around plus and minus 1 of the I prompt correlator. The visual investigation is further validated thanks the PLI/TTL approach, where in the case (a) the lock condition is not satisfied while 100 ms of time to lock obtained with 1 Hz bandwidth. Therefore, the previously commented outcomes demonstrates and shows what argued before regarding the beneficial effect of reducing the bandwidth when the conditions are weaker.
However, the best compromise to our analysis is represented by 10 Hz that guarantees a tolerance against the dynamic stress and a possibility to face relatively low C/N0.

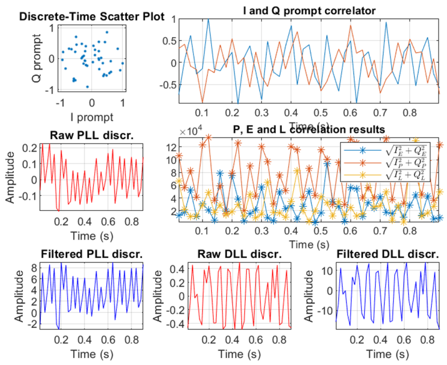

(a) $B_{PLL} = 15$ Hz

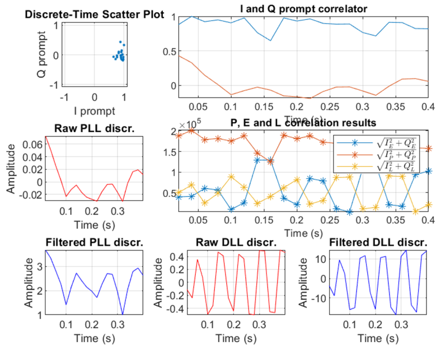

(b) $B_{PLL} = 10$ Hz

Figure 4.3: Comparison of the tracking results of a 1s GAL E1c signal with C/N0 = 38 dB-Hz for different PLL bandwidth.

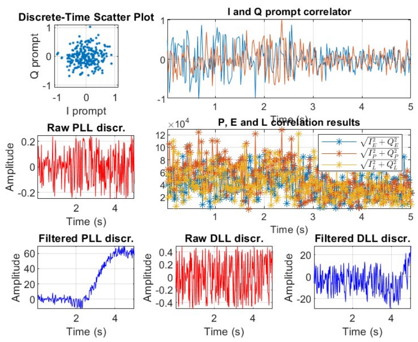

(a) $B_{PLL} = 10$ Hz

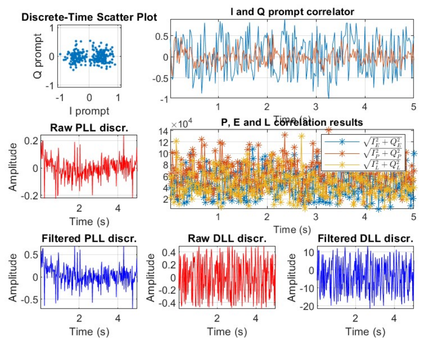

(b) $B_{PLL} = 1$ Hz

Figure 4.4: Comparison of the tracking results of a 5s GPS L1 signal with C/N0 = 24 dB-Hz for different PLL bandwidth.

4.3.2 Tracking performance versus the integration time

A simulation with varying C/N0 ratios is suggested as a method for locating an appropriate value for the integration time. The carrier loop bandwidth is kept constant at 10 Hz, and an integration time of 1 millisecond and 20 milliseconds is tested for values of C/N0 ranging from 24 to 38 dB-Hz. As with the Qascom snapshots, the duration of the signal that is being considered is one second. As can be seen in the Figure 4.5, for values of C/N0 greater than or equal to 30 dB-Hz, we are able to track the most powerful satellite with either value of integration time. However, an integration time of 1 millisecond is insufficient to work at C/N0 values lower than 30 dB-Hz. This is due to the fact that shorter values of integration result in a higher level of noise being applied to the estimated parameters. Therefore, in a condition of lower values C/N0 an integration time of 1 ms is not enough to make the tracking converges.
Conversely, with an integration time of 20 ms, we are able to track the signal up to a C/N0 of 24 dBHz. There is a problem brought on by the high value of the integration time. It makes the tracking less robust against high-dynamics. However, the dynamic stress does not represent a big issue in our case since we are analysing a very brief signal, so that the time window over which the Doppler can change is reduced and it appears to be constant. As a result, we can reach the conclusion that an integration time of 20 milliseconds might be an acceptable trade-off in order to keep track of the IQ samples that are provided by the receiver.

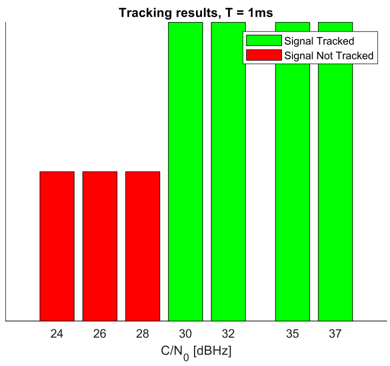

(a) Tcoh = 1 ms

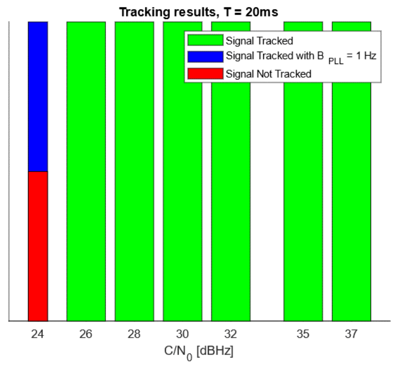

(b) Tcoh = 20 ms

Figure 4.5: Tracked GPS L1 satellite for different C/N0 with and without time extension.

4.3.3 Tracking performance depending on the E-L spacing

The DLL is based on the correlation of the incoming signal with two replicas of the local code, known as the early replicas and the late replicas, as was previously discussed in section 1.5.2. The spacing indicated as Δ is the spacing between the early and late correlator. The noise at the input of the DLL is directly proportional to the E-L spacing, hence the greater the spacing between the early and late correlator, the higher the noise contribution on the loop.

During the course of our investigation, we examined whether or not there would be a positive impact if the distance between components was made smaller in a space scenario. The simulation was performed on IQ samples at 45RE and 60RE taken from the Qascom data-set.

Figure 4.6 and Figure 4.7 display the comparison between two tracking outputs obtained processing the same signal but changing the spacing from 1 code period to one-fifth of the code period. The signals under test are one of the Qascom data-set IQS at 45RE and 60RE respectively. We can observe that in both situation not particular gain in terms of tracking performances comes out. At 45 RE, the tracking is not able to converge with a spacing equal to one chip and even if it is reduced, the situation remains unchanged. Therefore, the spacing reduction is not able to make the tracking to converge.

Differently, at 60 RE, we are able to achieve the lock condition. A value of Δ of one-fifth of the code period was tested trying to reduce time to reach the tracking convergence. However, the TTL obtained remains the same and the only beneficial effect that was observed was that the DLL outcomes became less noisy.

As a result, because we want to minimise the TTL value, the value of the E-L spacing does not have significant impact on our analysis.

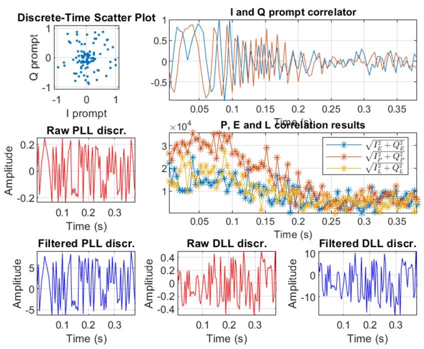

(a) $\Delta = T_c$

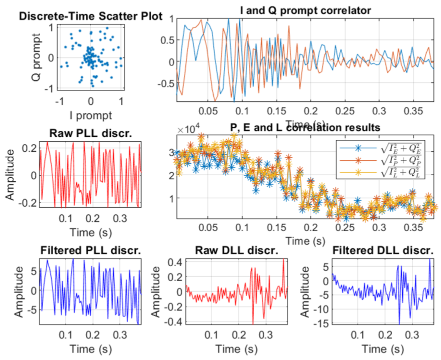

(b) $\Delta = 0.2T_c$

Figure 4.6: Comparison of the tracking results of a 1s GPS L1 signal at 45RE for different spacing.

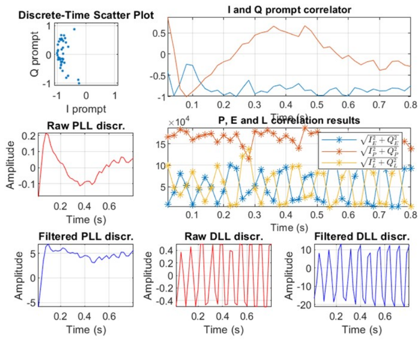

(a) $\Delta = T_c$

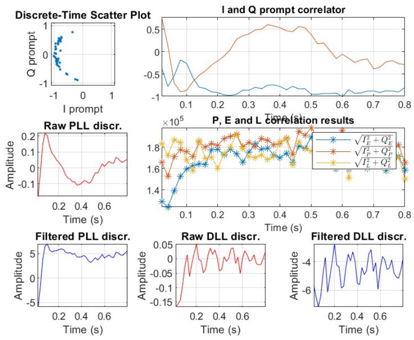

(b) $\Delta = 0.2T_c$

Figure 4.7: Comparison of the tracking results of a 1s GPS L1 signal at 60RE for different spacing.

4.3.4 Tracking performance optimizing the FLL-PLL architecture

As already discussed in section 1.5.1, the PLL processing is typically preceded by the FLL constituting an FLL-assisted-PLL carrier tracking loop. The reason behind that must be explained introducing a new tracking paradox. In fact, to tolerate dynamic stress the discriminator must be an FLL, but on the other hand, a PLL discriminator is needed to be robust against the noise. In practice the compromise is to use a PLL based loop assisted by an FLL so that the system is able to employ the benefits of both architecture. The FLL provides a more accurate value of frequency allowing the PLL to work on a narrow band which results in a shorter transient time.
To return back to our analysis, given that the signal is very short, the problem stands on how to set the FLL duration. The time over which the FLL is run is subtracted by the total tracking time, in other words the TTL must be at least the FLL duration, given that no lock can be achieved during the frequency adjustment. The duration must be set so that the FLL gives to the PLL a starting Doppler frequency accurate enough to allow the tracking lock. It can be viewed as a further adjustment of the rough estimation of the Doppler given by the acquisition. Therefore an other trade-off arises. A large FLL duration means a faster convergence of the PLL, but could means an higher value of TTL depending on the situation.
Note that if an external aiding is present, the FLL duration could be reduced or even removed further decreasing the TTL values.
Various simulations was performed in different conditions: using only the PLL, using the FLL-assisted-PLL and varying the FLL duration trying to figure out what the optimal value is.
Figure 4.8 and Figure 4.9 show the comparison of two tracking outputs, with and without the frequency-locked loop respectively at 45RE and 60RE distances. Each picture depicts the changes in the values of correlator outputs $Q_{k,d/p}, I_{k,d/p}$, raw and filtered PLL discriminator output $\delta\varphi_k$, prompt, early and late correlator results and raw and filtered DLL discriminator output. The signals under test are respectively a Galileo E1c and a GPS L1 simulated provided by Qascom.
We can notice that in both situations the lock condition is not satisfied when the FLL is not employed. The points of the scatter plots shows a rotating trend even if the prompt, the early and the late correlator are displaced in the correct way. This is the typical situation where the phase rotates due to a not accurate starting frequency value that can be improved by means of the FLL assistance. It is more evident in the first situation at 45RE. As a matter of fact, in either circumstance adding an FLL of 300 ms duration, the lock is achieved after 100 ms with an overall TTL of 400 ms. The scatter points at 45RE converge to -1 since in Galileo E1c signal is a pilot, while the GPS one normally converge to plus and minus one since the signal contains the navigation message.
Note that even the FLL has its own bandwidth that is fixed to 15 Hz following analogue considerations discussed during the design of the PLL bandwidth. In conclusion, a brief

assistance of FLL is recommended in any situation to process the space IQ samples, and the exact value should be fixed post-processing in an efficient manner for each individual signal in accordance with the value of the Doppler shift and the C/N0.

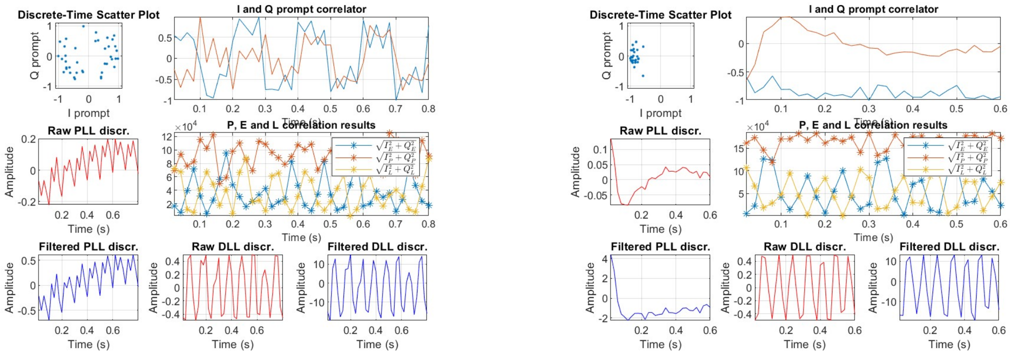

(a) No FLL

(b) FLL duration = 300ms

Figure 4.8: Comparison of the tracking results of a 1s GAL E1c signal at 45RE for different FLL duration.

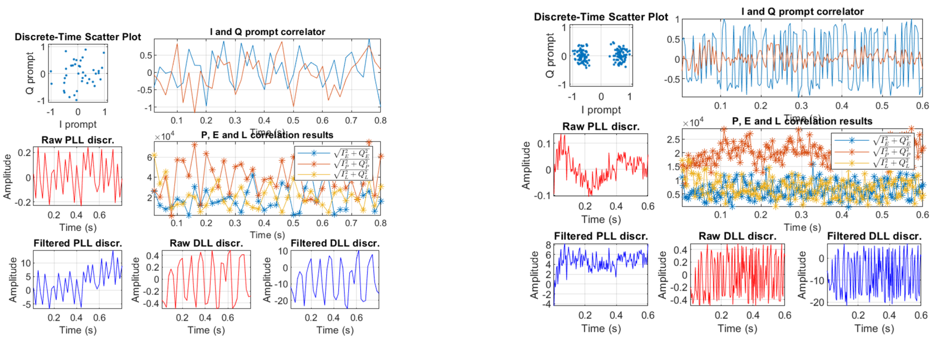

(a) No FLL

(b) FLL duration = 300ms

Figure 4.9: Comparison of the tracking results of a 1s GPS L1 signal at 60RE for different FLL duration.

4.3.5 Tracking performance depending on the size of Doppler frequency bins

The Doppler frequency is the resolution through which the Doppler is evaluated in the search space of the acquisition (see Chapter 1). Consequently, this parameter does not affect directly the tracking output, but, it could allows to start from a more precise value of the Doppler in the tracking stage. The possibility to increase the resolution in the software receiver could mimic an external aiding giving us a better estimation of the Doppler in a real receiver scenario. Starting from a better value of the Doppler allows to minimize the FLL time needed to reach the tracking lock. As a matter of fact, since the FLL tries to converge to the correct value of the Doppler, it requires less time if the starting point is more near to the "right" value. If the FLL time is reduced, the overall TLL is reduced as well meaning that the time required to achieve the lock is minimized.

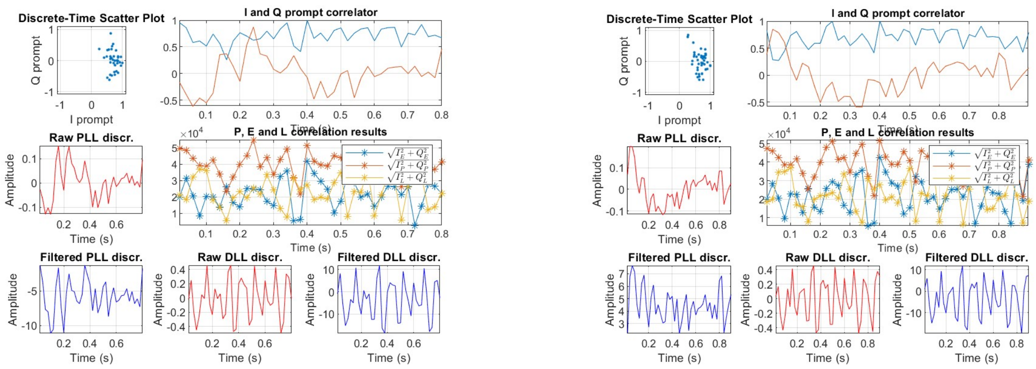

(a) Doppler Step = 50 Hz

(b) Doppler Step = 10 Hz

Figure 4.10: Comparison of the tracking results of a 1s GPS L1 signal at 45RE for different Doppler frequency bins.

Two different simulations are proposed (Figure 4.10 and Figure 4.11) one for GPS L1 Qascom signal and the other for GAL E1c. Table 4.4 summarizes the results, reporting the TTL values obtained during the simulations. We can observe that for the GPS signal, the increase of resolution on the Doppler gives a better starting frequency to the tracking stage so that the time to lock is reduced from 500 ms with a resolution of 50 Hz to 150 ms with a resolution of 10 Hz. However, in the second situation the tracking outputs are identical so that the TTL value remains the same. Therefore, in this particular situation, the Doppler frequency bins reduction does not provide any advantage since the Doppler provided by the Acquisition stage does not change. The conclusion is that an increase of Doppler resolution could be or beneficial or, in some situation, unnecessary, depending on the signal under test.

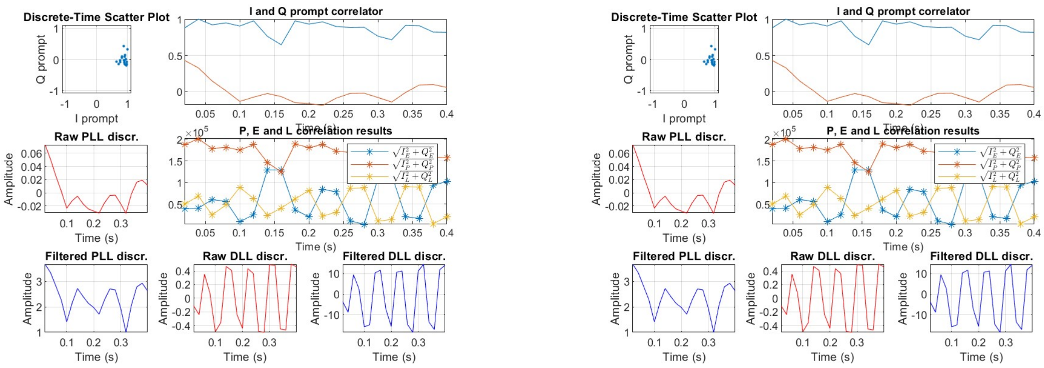

(a) Doppler Step = 100 Hz

(b) Doppler Step = 20 Hz

Figure 4.11: Comparison of the tracking results of a 1s GAL E1c signal at 45RE for different Doppler frequency bins.

DopStep [Hz]	**50 (GPS), 100 (GAL)**	**10 (GPS), 20 (GAL)**
TTL (GPS)	500 ms	150 ms
TTL (GAL)	120 ms	120 ms

Table 4.4: TTL values reducing the Doppler frequency bins.

4.4 IQS processing: Qascom signals results

After designing the tracking parameters, the data-sets provided by Qascom is entirely processed with the software receiver. The Data-sets consist on 1 signal at 30RE, 1 signal at 61RE (MSO), 2 signals at 45RE and 4 signals at 60RE with a total of 8 signals under investigation.
The parameters of the software receiver are summarized in Table 4.5 under the considerations taken in the previous sections. In Italics are reported the varying parameters meaning that more values was tested to find the set of these providing the best tracking results. The optimal set of the varying parameters depends on the specific signals so that it must be found specifically for each data-set.
The acquisition results and considerations have already been discussed in section 4.2.
Concerning the Tracking, the number of lock achieved processing the mentioned signals is 3 for GPS and 4 for Galileo with a total of 7 lock declarations.
The values of TTL corresponding to the lock are summarized in Table 4.6. To be more specific, the maximum, the mean and the minimum value of TTL are reported. The results indicate that with a signal duration of 200 ms, few signals can be tracked and if this value growths to 400 ms the lock is achieved for a large number of signals. We can suppose that

an order of magnitude of 300-400 ms of snapshot duration is the minimum needed to hope to track at least one satellite during the mission. It is important to underline that this duration allows the initial assistance of the FLL that is crucial in the most of the situation to track the signals. The number of lock obtained just employing a PLL drops from 7 to 1.
Further post-processing analysis can be performed trying to improve the results, even modifying the tracking architecture to be suitable against the space scenario (section 2.4). Furthermore, an external aiding as the Orbital filter can be used to retrieve information about the Doppler and reduce and even remove the initial assistance of the FLL leading to a further improvement.

Parameter	**GPS**	**GAL**
Tcoh Acquisition	10 ms	12 ms
n. of non-coherent accumulator	6	6
Doppler bin size	50 Hz	100 Hz
False Alarm Probability	1e-3	1e-3
DLL Bandwidth	10 Hz	10 Hz
PLL order	3	3
PLI threshold	0.766	0.766
DLL Correlator Spacing	0.2-1 chip	0.2-1 chip
Tcoh Tracking	4-20 ms	4-20 ms
PLL bandwidth	1-10 Hz	1-10 Hz
FLL duration	0-400 ms	0-400 ms

Table 4.5: Receiver Configuration. Varying parameters in Italics.

Minimum TTL	80 ms
Average TTL	335 ms
Maximum TTL	500 ms

Table 4.6: Time to lock values obtained during the simulations.

4.5 IQS Processing: Montecarlo simulation

The second part of the experiments is devoted to a Montecarlo simulation performed to investigate the impact of the signal parameters on the tracking performances. To be more specific, the parameters analyzed are the sampling frequency and the number of quantization bits of the signals. The impact of these parameters on our analysis can be essential, since there is a direct dependence with the data volume of the IQS. In fact, the larger the value of the sampling frequency the larger is the data volume of the snapshot fixed the signal duration since more samples are saved. An analogue discussion can be repeated for the quantization bits. If the number of quantization bits increases, the IQS data volume increases as well. A practical example of the mentioned trend is depicted by the figure 4.12 for a specific case of IQS duration of 300 ms. The IQS data volume

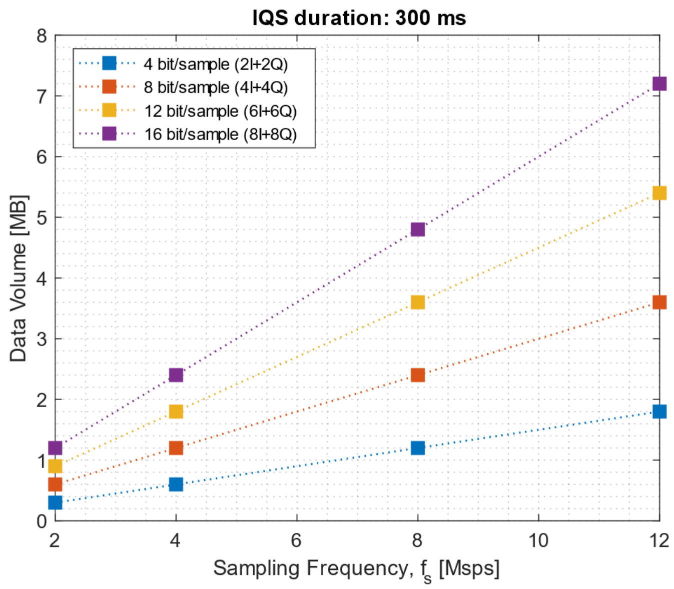

Figure 4.12: IQS data volume versus the sampling frequency for different number of quantization bits.

is limited by the agreement limitations, thus it should be reduced as possible. The aim of the following analysis is to investigate the trade-off between the quality and the length of the signal. Understand if it is convenient having a signal with more samples and more bits or a signal longer from a tracking point of view.

4.5.1 Impact of the Sampling frequency

The first analysis is devoted on understanding the impact of the sampling on the tracking performances. As mentioned before, if the sampling frequency is reduced, the data volume of the signal increases, hence the smaller is the duration of the signal available. For these reasons, it can be very useful to analyze the tracking performances varying the value of the sampling frequency and trying to design an optimal value for the mission.
The values of the frequency tested are 4, 8 and 12 Msps, while the number of quantization bits is fixed to 8 based on that used for the IQS of Qascom. A first check of the simulation environment is done comparing the results on the IQS of Qascom with our generated signal. Given that analogue outputs are achieved we can conclude that the signal generation was

done correctly. Subsequently, a Montecarlo simulation is performed for each value of frequency and for different points of the receiver orbits: 45RE and 60RE. During the experiments the duration of the FLL is fixed to 200 ms. The outputs of the simulations are the TTL (already presented) and the Percentages of Lock (POL), key quantities to characterize the processing of the tracking stage. The TTL is obtained mediating the value of the TTL for each simulations only when lock is achieved, otherwise obviously no significant value of TTL can be computed. The POL is computed as the ratio between the case in which the lock was achieved and the total number of iteration of the simulation. The total number of iteration for each Montecarlo simulations is fixed to 1000 taking into account the empirical convergence of the variable at stake. In fact, Figure 4.13 depicts the mean of the TTL during the running of the experiment versus the number of lock achieved at that iteration. We can note that just after 200 lock the mean starts being stable since no significant fluctuations are present, then we can conclude that the number of iterations is enough to get a stable convergence of the mean. It is important to underline that the number of lock does not coincide with the total number of iterations since in some cases the tracking cannot achieve the lock condition. On this purpose, the variable POL is considered.

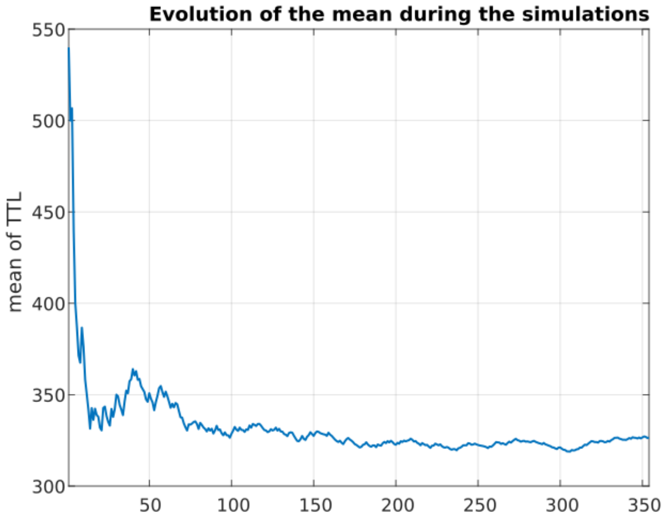

Figure 4.13: Evolution of the TTL mean during the simulation. In the x-axis the number of lock during the simulation.

As it can be expected, the results shows that the TTL decreases almost linearly with the sampling frequency while the POL increases, even if with a relative small value of slope in both cases (Figure 4.14 and Figure 4.15). In other words, we have a gain by increasing the sampling frequency on both the mean value of the time to get the lock and the total number of lock. Anyway, as said before, an higher sampling frequency means a lower duration of the IQS available. Therefore, a trade-off arises between the gain obtained in terms of tracking performances and a loss of data duration due to an higher frequency. For example, if the sampling frequency reduces from 8 to 4 Msps, the data volume decreases from 2.4 MB to 1.2 MB (fixed the IQS duration to 300ms). However, the tracking performances get worse, considering the case Galileo 60RE the POL drops from 30% to 24% and the TTL increases from 300 ms to 345 ms. Therefore, the design choice could be or having an IQS duration of 300 ms with 8 Msps of sampling frequency corresponding to a data volume of 2.4 MB or an IQS duration of 400 ms with 4 Msps which corresponds to a data volume of 2 MB. Based on this consideration the optimal choice seems to be the second one with 4 Msps since it ensures a lower value of data volume meaning that we are saving memory during the data collection. However, the presented example is just an approximation done for sake of simplicity , a more in-depth analysis is needed taking into account other parameters and signals during the real design phase.
Moreover, the pictures shows better results at 45RE than 60RE, since as already explained, the longer the distances the lower the C/N0.

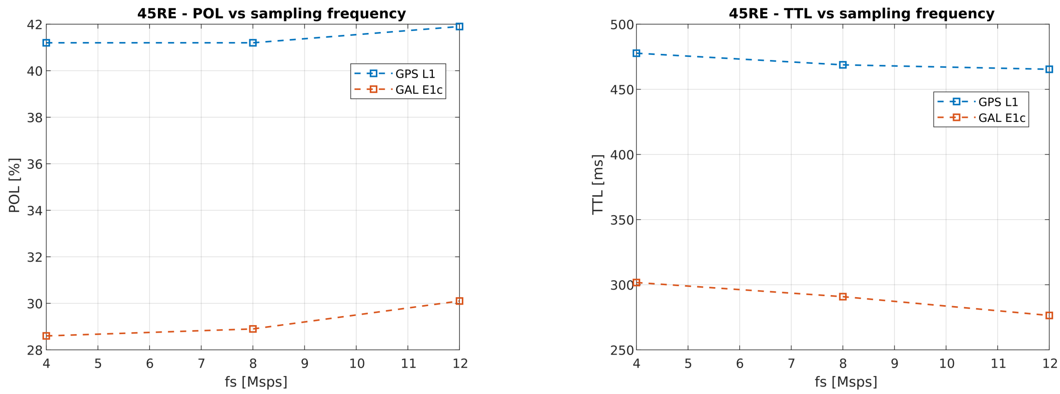

(a) POL versus fs **(b)** TTL versus fs

Figure 4.14: Sampling frequency analysis - 45RE

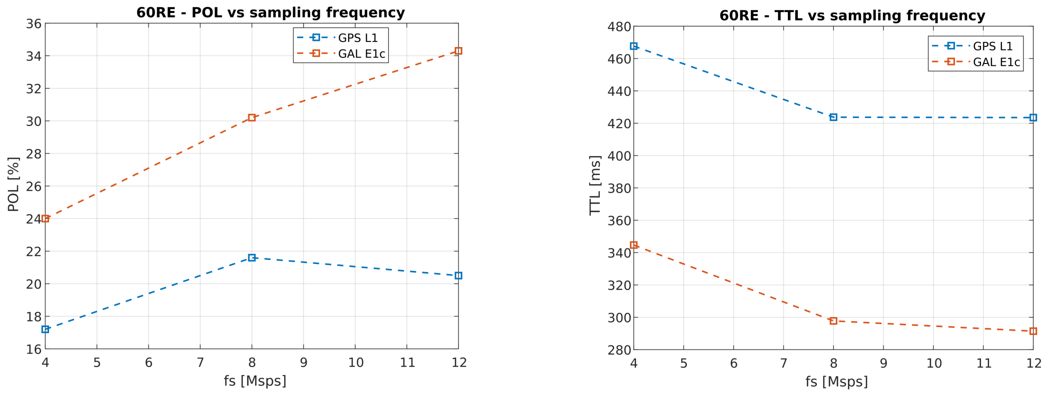

(a) POL versus fs **(b)** TTL versus fs

Figure 4.15: Sampling frequency analysis - 60RE

4.5.2 Impact of the number of Quantization bits

An analog analysis is repeated but now testing the impact of the number of quantization bits on the tracking performances, again in terms of POL and TTL. On this purpose, during this experiment the number of quantization bits antecedently fixed to 8, now takes the values of 4,6 and 8 bits, while the sampling frequency is fixed to 8 Msps. Therefore, a Montecarlo simulation is again proposed with a number of iterations equal to 1000 (as before) and testing 45RE and 60RE as distances. The FLL duration remains fixed to the value of 200 ms. Differently from the previous outcomes, the following results do not show a specific trend varying the number of quantization bits, rather, the tracking performances seems to be not affected by this changement since the TTL and POL values are basically constant during the variation as we can see from the figures. The same considerations can be repeated for both the distances considered. Consequently, this can suggest to reduce as possible the number of quantization bits since there are no reasons to maintain an higher level of quantization equal bits from a tracking point of view. Reducing the number of quantization bits, the data volume is reduced as well, granting the possibility to save memory that can be crucial to face the stringent constrains on the data storage during the mission. In conclusion, the results argue that is better having longer IQS than having IQS with an higher number of quantization bits.

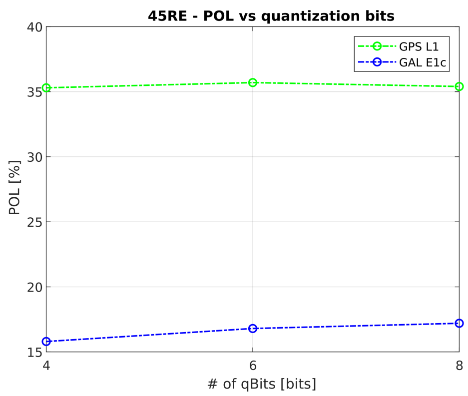

(a) POL versus q

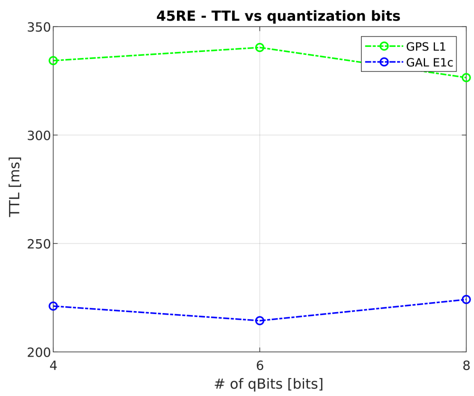

(b) TTL versus q

Figure 4.16: Quantization bits analysis - 45RE

4.5.3 Considerations on IQS duration

After discussing the impact of the IQ samples parameters, some considerations about IQS duration should be done. On this purpose, the Figure 4.17 and Figure 4.18 depict the histogram of TTL during the single experiment and the corresponding cumulative POL. The yellow line indicates the correct way to interpret the graph, that is to fix a value of TTL and looking on what is the percentages associated. In other words, fixing a value of TTL means practically fixing the value of the snapshot duration. To give an example, if we choose an IQS duration of 300 ms, then we will have 28% probability to achieve the tracking lock at 45RE on GPS L1. If we are able to record more ms up to 500 ms, the chances to track the GPS signal grows to 40%.
We can notice from the mentioned figures that some differences emerges on the distribution of the TTL between GPS and Galileo cases. To be more specific, the TTL distribution of GPS appears more widespread meaning that the TTL value is characterized by an higher variance. Conversely, TTL values of Galileo are distributed more intensely around one single value. The TTL mean value obtained with Galileo has then a lower variance.
It is important to underline that the results was obtained with an FLL duration fixed to 200 ms, so that the minimum TTL value obtainable is 200 ms.
Passing from a distance of 45RE to 60RE the results worsen, as expected, since the signal is characterized by a higher power noise level. For instance, the probability to achieve the lock with a duration of 400 ms drops from 36 % to 10 % in case of GPS signal. Similarly, the chances to track a Galileo signal reduces from 23 % to 15 % for a snapshot duration of 300 ms. However, the Galileo signal appears to be more robust against higher distances than GPS signal, since the impact on the POL is lighter. The reasons behind that are to be searched both in the proprieties of the signal and in the specific architecture and processing of our receiver. A further analysis needs to be done to properly answer the question.

Tables 4.7 and 4.8 summarizes the results for sake of explanation reporting the probability to track at least one signal (GPS or Galileo) for different values of snapshot duration designed. The proposed probability is computed summing the probability to track a GPS satellite with a probability to track a Galileo satellite, since it represents the chance to track at least one signal belonging to one of the two constellation. To this sum must be subtracted the intersection of the two events following the union rule for probability formula:

$$P(A \cup B) = P(A) + P(B) - P(A \cap B) = P(A) + P(B) + P(A)P(B) \tag{28}$$

If the two events are statistically independent the probability of the intersection event can be computed simply as the product between the probability to obtain the two events.
The results are quite encouraging, they indicate that with a time window ensuring to collect at least 300 ms of data, the possibility to achieve a successfully tracking are 45 % at 45RE and nearly 20 % at 60RE. If the length of the snapshots collected is enlarged to

400 ms, the probability increase to 51 % and 30 % respectively. Conversely, if the IQS duration obtainable is in the order of 250 ms, the chances drop to 28 % at 45RE and only 4 % at 60RE. This suggests the need to collect at least 300 ms duration of data to hope to achieve a successful tracking. This can be explained by the fact that an FLL duration of 200 ms seems to be the minimum value granting the possibility to pull aside the signal. It is important to underline that this are just preliminary results, obtained taking just one set of the receiver parameters for each realization. Therefore, they represents a sort of worst case given that when the real collected data will be available, for each of that the enormous flexibility of the software receiver can be exploited to process them. To go into details, for each IQS under test different both acquisition and tracking stage can be optimized, varying the parameters or the architecture itself with a more advanced and sophisticated one. For example, once that the signal is successfully acquired, the information about the Doppler and Delay can be exploited to reprocess the signal reducing strongly the search space centred at that values. This could lead to a more accurate acquisition estimation that is then passed as a starting point of the tracking. Moreover, the tracking stage can be improved increasing the order of the filters or optimizing thanks repeated test the value of the parameters as done in the first part of the chapter.

In conclusion, all of the presented results can be useful during the design of the IQS time window of the mission. The best trade-off must be found taking into account the mentioned considerations and the agreement limitations on the data storage and transmission.

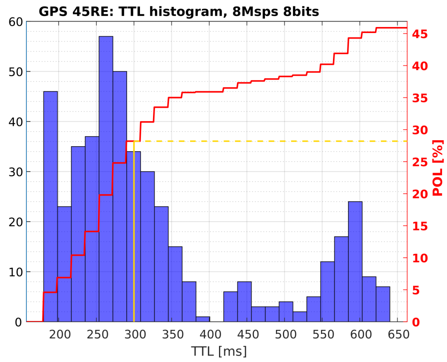

(a) GPS L1

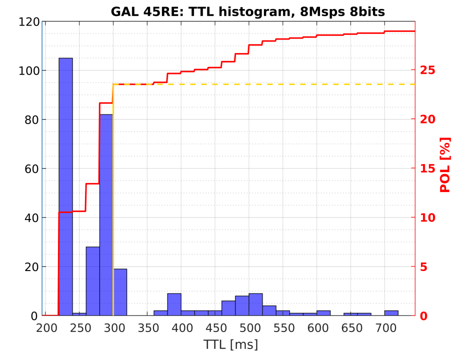

(b) GAL E1c

Figure 4.17: 45RE - TTL histogram and corresponding cumulative POL, 8 Msps of sampling frequency and 8 bits as number of quantization bits.

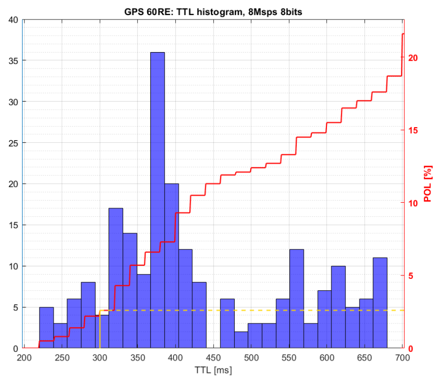

(a) GPS L1

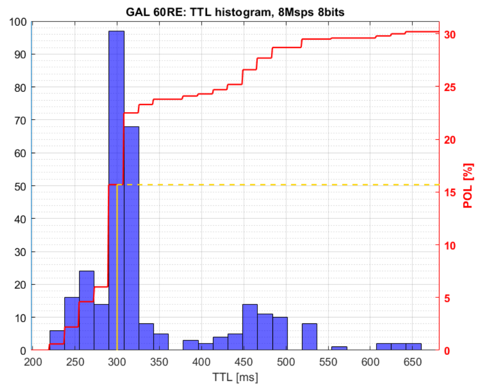

(b) GAL E1c

Figure 4.18: 60RE - TTL histogram and corresponding cumulative POL, 8 Msps of sampling frequency and 8 bits as number of quantization bits.

IQS duration	Probability to track the signal
250 ms	28 %
300 ms	45 %
400 ms	51 %
500 ms	55 %

Table 4.7: Probability to track the signal varying the IQS duration at 45RE.

IQS duration	Probability to track the signal
250 ms	4 %
300 ms	18 %
400 ms	30 %
500 ms	36 %

Table 4.8: Probability to track the signal varying the IQS duration at 60RE

Chapter 5

Conclusions

The use of in-orbit Global Navigation Satellite Systems (GNSS) receivers has been experimentally validated within the Space Service Volume (SSV), at LEO and MEO altitudes as well as up to GEO altitudes. Latest missions, then, have unveiled GNSS performance for distances of about 150,000 km away from the Earth's surface. The study of Earth GNSS signal beyond such an altitude is still matter of research mostly based on modeling and extrapolation from the experience of using GNSS on the Earth and on lower orbits. The Lunar GNSS Receiver Experiment (LuGRE) is a joint NASA-Italian Space Agency (ASI) payload on the Firefly Blue Ghost Mission 1 with the goal to demonstrate GNSS-based positioning, navigation, and timing at the Moon. When launched in 2024, LuGRE will collect GPS and Galileo measurements in transit between Earth and the Moon, in lunar orbit, and on the lunar surface, and will conduct onboard and ground-based navigation experiments using the collected data. The receiver is able to provide, PVT solutions, the GNSS raw observables obtained by the real time operation, as well as snapshots of IF digital samples collected by the RF front-end at frequencies L1/E1 and L5/E5 for GPS and Galileo. These data will be the input for the different science investigations, that require then the development of proper analysis tools that will be the core of the ground segment during the mission. The current work done by the science team of NASA and ASI, which is supported by a research team at Politecnico di Torino, is planning the data acquisitions during the time windows dedicated to the LuGRE payload in the checkout, transit and surface mission phases.
The reasons to extend the GNSS domain to high-Earth orbit and in lunar space are several. For example, spacecraft can use the GNSS signals to obtain PVT information which is critical to mission operation without the need for an onboard clock. This grants to reduce tracking and operational cost.

This thesis work aims at investigating the possibility to acquire and track the snapshot of a given duration. In this way, a contribution can be provided to to planning the time windows dedicated to the snapshots collection as well as designing their duration. The first

step was to study and implement techniques allowing to increase the sensitivity of GNSS space-born receivers in order to process the very weak signals in non-terrestrial applications. Advanced techniques as coherent and non coherent time extension are proposed and employed to face the with low carrier-to-noise density ratio, increasing the robustness of the acquisition stage.
The signals at these distances are not available, since no receiver has ever reached such heights. Therefore, the snapshots was simulated both by Qascom and our team by proper modelling the space environment thanks to information about the trajectories and the antennas. Finally, the simulated signals was processed with the software receiver applying the high sensitivity techniques previously mentioned. Thanks to that, the receiver was able to acquire the weak signal with an order of magnitude of just 100 ms, suggesting that this duration is enough to perform the acquisition stage. Conversely, the tracking proved to be more difficult and required a more in-depth analysis. On this direction, a first processing was performed in order to optimize as possible the tracking parameters to cope with this harsh environment. Therefore, a Montecarlo simulation was executed to provide the probabilities to obtain a successful tracking on a snapshot with a given length and to investigate the impact of the sampling frequency and the number of quantization bits on the tracking performances. The results shows that the performance slightly worsen by reducing the sampling frequency, while no significant trend emerged varying the number of quantization bits. The latter can be then reduced without impacting on the performances and granting to obtain a longer signal duration.
Moreover, the results highlights the need to have at least 300 ms of data collected, since under this duration the chances to achieve the tracking lock drop drastically. To conclude, the accomplished results and considerations can be exploited during the design of the IQS time window of the mission. The best trade-off must be found taking into account the mentioned considerations and the agreement limitations on the data storage and transmission.

Bibliography

[1] EUSPA - *What is GNSS?* [online]. 2021. URL: https://www.euspa.europa.eu/european-space/eu-space-programme/what-gnss (cit. on p.3)

[2] GPS.gov. *Space Segment.* Official U.S. government information about the Global Positioning System (GPS). [online]. URL: https://www.gps.gov/systems/gps/space/ (cit. on p. 3).

[3] ESA - Navipedia. *GLONASS Space Segment.* [online]. URL: https://gssc.esa.int/navipedia/index.php/GLONASS_Space_Segment (cit. on p. 4).

[4] ESA - Navipedia. *Galielo Space Segment.* [online]. URL: https://gssc.esa.int/navipedia/index.php/Galielo_Space_Segment (cit. on p. 4).

[5] ESA - Navipedia. *BeiDou Space Segment.* [online]. URL: https://gssc.esa.int/navipedia/index.php/BeiDou_Space_Segment (cit. on p. 4).

[6] GISGeography. *How GPS Receivers Work – Trilateration vs Triangulation.* [online] URL: https://gisgeography.com/trilateration-triangulation-gps/#:~:text=Trilateration (cit. on p. 5).

[7] I. Sharp, K. Yu and Y. J. Guo, "GDOP Analysis for Positioning System Design," in IEEE Transactions on Vehicular Technology, vol. 58, no. 7, pp. 3371-3382, Sept. 2009, DOI: 10.1109/TVT.2009.2017270 (cit. on p. 5).

[8] N. Blanco-Delgado, F. D. Nunes and G. Seco-Granados, "Relation between GDOP and the geometry of the satellite constellation", 2011 International Conference on Localization and GNSS (ICL-GNSS), 2011, pp. 175-180, DOI: 10.1109/ICL-GNSS.2011.5955282 (cit. on p. 5).

[9] ESA - Navipedia. *GNSS signal.* [online]. URL: https://gssc.esa.int/navipedia/index.php/GNSS_signal (cit. on p. 6).

[10] ESA - Navipedia. *Galileo Signal Plan.* [online].
URL: https://gssc.esa.int/navipedia/index.php/Galileo_Signal_Plan (cit. on p. 10).

[11] ESA - Navipedia. *Delay Lock Loop (DLL)*. [online]. URL: https://gssc.esa.int/navipedia/index.php/Delay_Lock_Loop_(DLL) (cit. on p. 20).

[12] ESA - Navipedia. *Phase Lock Loop (PLL)*. [online]. URL: https://gssc.esa.int/navipedia/index.php/Phase_Lock_Loop_(PLL) (cit. on p. 23).

[13] Marco Rao and Gianluca Falco. ≪How can pseudorange measurements be generated from code tracking≫. In: Inside GNSS Mag 7 (2012), pp. 26–33 (cit. on p. 24).

[14] NASA - Space communications.
NASA Explores Upper Limits of Global Navigation Systems for Artemis. [online]. URL: https://shorturl.at/ain69 (cit. on p. 28).

[15] United Nations Office for Outer Space Affairs. ≪Interoperable GNSS space service volume≫. In: The Interoperable Global Navigation Satellite Systems Space Service Volume. United Nations, 2019, pp. 7–10 (cit. on p. 25).

[16] Thornton, Catherine and Border, James (2003).
≪Radiometric Tracking Techniques for Deep-Space Navigation≫. DOI: 10.1002/0471728454. (cit. on p. 25).

[17] Franzese, Vittorio, Pierluigi Di Lizia, and Francesco Topputo. "Autonomous optical navigation for lumio mission." 2018 Space Flight Mechanics Meeting. 2018. DOI: 10.2514/6.2018-1977 (cit. on p. 25)

[18] Xiaolin, Ning, et al. "Pulsar navigation using time of arrival (TOA) and time differential TOA (TDTOA)." Acta Astronautica 142 (2018): 57-63. DOI: 10.1016/j.actaastro.2017.09.039 (cit. on p. 25)

[19] Frank Stephen Tromp Van Diggelen. *A-gps: Assisted gps, gnss, and sbas*. Artech house, 2009 (cit. on p. 30)

[20] Vincenzo Capuano, Paul Blunt, Cyril Botteron, and Pierre-André Farine. ≪Orbital Filter Aiding of a High Sensitivity GPS Receiver for Lunar Missions≫. In: Jan. 2016. DOI: 10.33012/2016.13422 (cit. on p. 33).

[21] Vincenzo Capuano, Paul Blunt, Cyril Botteron, Jia Tian, Jérôme Leclère, Yanguang Wang, Francesco Basile, and Pierre-André Farine. ≪Standalone GPS L1 C/A receiver for lunar missions≫. In: Sensors 16 (Mar. 2016), p. 347. DOI: 10.3390/s16030347 (cit. on p. 33).

[22] L. Musumeci, Fabio Dovis, João Silva, P.F. Silva, and Hugo Lopes. ≪Design of a High Sensitivity GNSS receiver for Lunar missions≫. In: Advances in Space Research 57 (Mar. 2016). DOI: 10.1016/j.asr.2016.03.020 (cit. on p. 33).

[23] Vincenzo Capuano. ≪GNSS-based Orbital Filter for Earth Moon Transfer Orbits≫. In: Journal of Navigation (Oct. 2015) (cit. on p. 33).

[24] P.F. Silva et al. ≪Weak GNSS signal navigation to the moon≫. In: vol. 4. Sept. 2013 (cit. on p. 33).

[25] Kaplan, E. D. (2006). *Understanding Gps: Principles and applications.* Artech House. (cit. on p. 31)

[26] F. van Graas, A. Soloviev, M. Uijt de Haag and S. Gunawardena, "Closed-Loop Sequential Signal Processing and Open-Loop Batch Processing Approaches for GNSS Receiver Design," in IEEE Journal of Selected Topics in Signal Processing, vol. 3, no. 4, pp. 571-586, Aug. 2009, DOI: 10.1109/JSTSP.2009.2023350 (cit. on p. 33).

[27] U. Cheng, W. J. Hurd, and J. I. Statman, "Spread spectrum code acquisition in the presence of Doppler shift and data modulation," IEEE Trans. Commun., vol. 38, no. 2, pp. 241–250, Feb. 1990 (cit. on p. 33).

[28] A. J. R. M. Coenen and D. J. R. van Nee, "Novel fast GPS/GLONASS code-acquisition technique using low update-rate FFT," Electron. Lett., vol. 28, no. 9, Apr. 1992. (cit. on p. 33).

[29] ISECG. *International Space Agencies Meet to Advance Coordination in Space Exploration of Moon and Mars.* [online]. URL: https://www.globalspaceexploration.org/ (cit. on p. 37).

[30] NASA - Artemis. *WHY WE ARE GOING TO THE MOON.* [online]. URL: https://www.nasa.gov/specials/artemis/ (cit. on p. 40).

[31] NASA - LuGRE presentation. *GNSS to the Moon.* [online] URL: https://www.gps.gov/cgsic/meetings/2021/ashman.pdf (cit. on p. 40).

[32] Parker, Joel J.K., Dovis, Fabio, Anderson, Benjamin, Ansalone, Luigi, Ashman, Benjamin, Bauer, Frank H., D'Amore, Giuseppe, Facchinetti, Claudia, Fantinato, Samuele, Impresario, Gabriele, McKim, Stephen A., Miotti, Efer, Miller, James J., Musmeci, Mario, Pozzobon, Oscar, Schlenker, Lauren, Tuozzi, Alberto, Valencia, Lisa, "The Lunar GNSS Receiver Experiment (LuGRE)," Proceedings of the 2022 International Technical Meeting of The Institute of Navigation, Long Beach, California, January 2022, pp. 420-437. URL: https://doi.org/10.33012/2022.18199 (cit. on p. 40).

[33] European GNSS Agency (GSA). *Power-efficient positioning for the Internet of Things.* Luxembourg: Publications Office of the European Union, June 2020. DOI: 10.2878/437669 (cit. on p. 43).

[34] V. Lucas-Sabola et al. “Efficiency Analysis of Cloud GNSS Signal Processing for IoT Applications”. In: Proceedings of the 30th International Technical Meeting of The Satellite Division of the Institute of Navigation (ION GNSS 2017) (Mar. 2017). DOI: 10.33012/2017.15237 (cit. on p. 43).

[35] Caner Savas, Gianluca Falco and Fabio Dovis. ”A Comparative Performance Analysis of GPS L1 C/A, L5 Acquisition and Tracking Stages Under Polar and Equatorial Scintillations”. In: Feb. 2021. DOI: 10.1109/TAES.2020.3011999 (cit. on p. 18).